# STUDY ON NONLINEAR CONVECTIVE FLOW OF HYBRID NANOFLUIDS IN AN ANNULUS

*PhD Synopsis submitted to CHRIST (Deemed to be University)*

*as partial requirement for the award of the Degree of*

**DOCTOR OF PHILOSOPHY**

**IN**

**MATHEMATICS**

by

THRIVENI K (1881513)

Research Scholar

Under the Supervision of

B Mahanthesh

Assistant Professor

Department of Mathematics

Signature of Scholar Signature of Supervisor

CENTER FOR RESEARCH

CHRIST (Deemed to be University)

BENGALURU

JUNE, 2021

## CENTRE FOR RESEARCH

### Approval of PhD Synopsis

[as per clause 11(k.) of CU Regulation for the Degree of Doctor of Philosophy, May 2019]

| | |
|---|---|
| Name of Scholar: | Thriveni K |
| Department: | Mathematics |
| Name of Supervisor: | B Mahanthesh |
| Names of Research Advisory Committee:<br>1. Dr B Mahanthesh<br>2. Dr Arun Kumar N<br>3. Dr Manjunatha S | |
| Name and Designation of External Reviewer if applicable: | |
| Date of Synopsis Presentation: | |
| Title of the PhD thesis: | Study on nonlinear convective flow of hybrid nanofluids in an annulus |
| Approved by:<br>1. Name of Supervisor: Dr B Mahanthesh Signature:<br>2. Name of RAC Member: Dr Arun Kumar N Signature:<br>3. Name of RAC Member: Dr Manjunatha S Signature:<br>4. Name of External reviewer (if applicable) Signature: | |

Head of Department:

---

Date of approval by Doctoral Committee:

Director Centre for Research

## ABSTRACT

In this modern fluid field technology, hybrid nanoliquids are of great interest to researchers due to their improved thermal properties which provide a superior improvement in heat transfer compared to nanoliquids. The hybrid nanoliquid flow in an annular geometry finds its relevance in engineering and material manufacturing processes such as heat exchangers, nuclear power plants, hot rolling, and heat storage systems due to their high heat transport rate. Since these devices are operated at moderate and very high temperatures adopting linear Boussinesq approximation becomes inappropriate. Owing to this, the present research is devoted to the study of flow, heat, and mass transport characteristics of hybrid nanofluid in an annulus including the effects of radial/transversal magnetic field, thermal radiation, exponential space-related heat source, uniform/non-uni--form heat source and variable thermophysical properties under the nonlinear Boussinesq approximation. The fundamental equations are obtained from the laws of conservation of mass, momentum, and energy. The dimensionless governing nonlinear equations are treated analytically/numerically (by employing shooting technique, finite difference method). Further, the sensitivity analysis using response surface methodology (RSM) is performed to enhance the understanding of heat and mass transport behavior. The significance of various flow parameters (involving in the problem) on the flow structure, thermal model, concentration field, heat, and mass transport rate are analyzed through 2D/3D-surface plots and discussed quantitatively.



**Key Words:** Annulus; Hybrid nanofluid; Nonlinear Boussinesq approximation; Response surface methodology; Sensitivity analysis.

# Contents

**1 INTRODUCTION** **1**

**2 NEED FOR THE STUDY** **6**

**3 OBJECTIVES OF THE STUDY** **6**

**4 METHODOLOGY, RESULTS: OVERVIEW OF THE RESEARCH WORK CARRIED OUT** **7**

4.1 PROBLEM 1: Nonlinear convective flow of hybrid nanofluid in an annulus with linearized thermal radiation . . . . . 7

4.1.1 Parametric Analysis . . . . . 12

4.1.2 Statistical Analysis . . . . . 13

4.1.3 Results . . . . . 13

4.2 PROBLEM 2: Nonlinear convective flow of hybrid nanofluid in an annulus with nonlinear thermal radiation . . . . . 14

4.2.1 Parametric Analysis . . . . . 17

4.2.2 Statistical Analysis . . . . . 18

4.2.3 Results . . . . . 22

4.3 PROBLEM 3: Nonlinear convective flow of hybrid nanofluid in an annulus with quadratic thermal radiation and variable fluid properties . . . . . 22

4.3.1 Parametric Analysis . . . . . 25

4.3.2 Statistical Analysis . . . . . 26

4.3.3 Results . . . . . 28

4.4 PROBLEM 4: Nonlinear convective flow of hybrid nanofluid in an annulus with an induced magnetic field . . . . . 29

4.4.1 Parametric Analysis . . . . . 31

4.4.2 Statistical Analysis . . . . . 33

4.4.3 Results . . . . . 34

4.5 PROBLEM 5: Nonlinear convective flow of hybrid nanofluid with temperature and space dependent internal heat sources . . . . . 35

4.5.1 Parametric Analysis . . . . . 37

4.5.2 Statistical Analysis . . . . . 37

4.5.3 Results . . . . . 38

4.6 PROBLEM 6: Flow of hybrid nanomaterial in an annulus using modified Buongiorno model . . . . . 41

4.6.1 Parametric Analysis . . . . . 44

4.6.2 Statistical Analysis . . . . . 45

4.6.3 Results . . . . . 45

**5 STRUCTURE OF THE DISSERTATION** **49**

**6 FUTURE RESEARCH WORK** **49**

**REFERENCES** **50**

**LIST OF PUBLICATIONS** **54**

**LIST OF PRESENTATIONS** **55**

# 1 INTRODUCTION

Fluid mechanics is the branch of applied mechanics which is concerned with the statics and dynamics of liquids and gases. Analysis of the fluid behavior is based upon the fundamental laws of applied mechanics that relate to the conservation of mass, energy, and momentum. Fluid dynamics is an important and rich branch of science and engineering, as every living in the universe has existed because of fluid. In fluid mechanics, especially fluid dynamics is an active field of research with many unsolved or partly solved problems. Fluid dynamics branches out into several sub-disciplines itself, including aerodynamics and hydrodynamics which play an important role in nature and technical applications. The study of the motion of fluids that can be approximated as incompressible such as liquids, especially water, and gases at low speed is usually referred to as hydrodynamics. A subcategory of hydrodynamics is hydraulics, which deals with liquid flows in pipes and open channels. Gas dynamics deals with the flow of fluids that undergo significant density changes, such as the flow of gases through nozzles at high speeds. The category aerodynamics deals with the flow of gases over bodies such as aircraft, rockets, and automobiles at high or low speeds. Some other specialized categories such as meteorology, oceanography, and hydrology deal with naturally occurring flows. Fluid mechanics is widely used both in everyday activities and in the design of modern engineering systems from vacuum cleaners to supersonic aircraft. Fluid mechanics also play a vital role in the human body. The heart is constantly pumping blood to all parts of the human body through the arteries and veins, and the lungs are the sites of airflow in alternating directions. All artificial hearts, breathing machines, and dialysis systems are designed based on fluid dynamics.

A body that is introduced into a fluid that is at a different temperature forms a source of equilibrium disturbance due to the thermal interaction between the body and the fluid. The reason for this process is that there are thermal interactions between the body and the medium. The fluid elements near the body surface assume the temperature of the body and then begin the propagation of heat into the fluid by heat conduction. This variation of the fluid temperature is accompanied by a density variation which brings about a distortion in its distribution corresponding to the theory of hydrostatic equilibrium. This leads to the process of the redistribution of the density which takes on the character of a continuous mutual substitution of fluid elements. In a particular case, when the density variation is caused by the non-uniformity of the temperatures is called thermal gravitational convection. When the motion and heat transfer occurs in an enclosed or infinite space then this process is called buoyancy convective flow. The convective mode of heat transfer is generally divided into two basic processes namely forced and natural/free convection. If the motion of the fluid arises from an external agent then the process is termed as forced convection. If there is no such externally induced flow is provided and the flow arises from the effect of a density difference, resulting from a temperature

or concentration difference, in a body force field such as the gravitational field, then the process is termed as natural or free convection. The density difference gives rise to buoyancy forces which drive the flow and the main difference between free and forced convection. Since, density is a function of temperature, concentration, and pressure it can be well explained with the help of the equation of state. In 1903 Boussinesq posted a mathematical model for vertical geometry by accounting body force. According to this approximation, the density in the linear momentum equation remains constant through the equation until it is multiplied with gravity. In the linear Boussinesq approximation (LBA), the fluctuation of density with temperature is taken as linear, which is obtained by truncating the density expansion of the Taylor series with temperature after the second term. This LBA holds good only if the temperature difference is very small. Some thermal systems such as solar collectors, combustions, nuclear reactors, and areas of reactor safety are operated at moderate and very high temperatures. In these cases, the temperature difference between the duct walls is significantly large, and the mathematical model developed with LBA becomes imprecise. Therefore, accounting nonlinear convection for fluid flow characteristics has more significance. Owing to this, in 1966 Goren [1] established the nonlinear density variation with temperature as $\triangle\rho = -\rho\beta(T - T_w)^2$. Later, Vajravelu and Sastri [2] studied the free convective flow between the two plates by considering both linear and quadratic fluctuation in the density with temperature as follows and it is termed as nonlinear Boussinesq approximation (NBA).

$$\Rightarrow \rho(T) = \rho(T_w) + \left(\frac{\partial\rho}{\partial T}\right)_w (T - T_w) + \frac{1}{2!}\left(\frac{\partial^1\rho}{\partial T^2}\right)_w (T - T_w)^2,$$

$$\Rightarrow \frac{\triangle\rho}{\rho} = -[\beta_0(T - T_w) + \beta_1(T - T_w)^2].$$

where $\beta_0 = \frac{1}{\rho}\left(\frac{\partial\rho}{\partial T}\right)_w$ and $\beta_1 = \frac{1}{2\rho}\left(\frac{\partial^2\rho}{\partial T^2}\right)_w$.

The quadratic convective flow in a porous wavy surface filled with nanoliquid was inspected by Kameswaran et al. [3]. Their results showed that an increase in nonlinear temperature causes an enhancement in the liquid velocity. Mahanthesh et al. [4] investigated the three-dimensional nonlinear convective flow of non-Newtonian nanofluid by accounting thermal radiation and NDT. They found that the temperature profile is stronger in the presence of NBA. Gireesha et al. [5] utilized the NBA to study the convective flow of nanoliquid subjected to an exponential heat source and variable viscosity. Their results showed that the thermophysical and cooling performance of base fluid can be controlled by nonlinear convection parameter. Vasu et al. [6] examined the transient flow of nanofluid over a sphere by accounting nonlinear Boussinesq approximation and they observed enhancement in heat and mass transport for an increase in nonlinear convection

parameter. Jha et al. [7] investigated the heat transfer past a plate subjected to the NBA and concluded that the velocity is higher in the presence of NBA than in the absence of the NBA.

The utility of most of the fluids as coolants has not been satisfactory due to their poor thermal conductivity. Improvement of heat transfer rate is a fundamental goal in many thermal management systems involving fluids as a working media, such as heat exchangers. In such systems, heat transfer enhancement has been attempted by the placement of fins, forced convection process through fans, ventilators, and other mechanisms. Even several decades ago attempts have been made by suspending micro-sized particles into the working liquids. This technique is also failed to boost heat transfer rate due to agglomeration of particles let to settling and abrasion of the surfaces on which they settled. A decade ago, Choi and Eastman [8] came up with an innovative technique of heat transfer enhancement which is suspending nanoparticles (particles with diameter 100nm) in working fluids. Nanoliquids are referred to as a mixture of nanoparticles and working liquids. The nanoparticles are typically made up of metals ($Al$, $Cu$), oxides ($Al_2O_3$, $CuO$, $TiO_2$, $SiO_2$), carbides ($SiC$), nitrides ($AlN$, $SiN$), or non-metals (graphite, single or multi-walled carbon nanotubes), and the working liquid is generally water, ethylene glycol, oil, lubricants, bio-fluids, polymer solutions, and kerosene. This enhancement in the heat transfer process is due to several reasons but the fundamental one is the high thermal conductivity of nanoparticles. Such thermal nanofluids for heat transfer applications represent a class of their difference from convectional colloids for other applications. There are three models to theoretically study the heat transfer enhancement using nanoliquids, they are:

1. Khanafer-Vafai-Lightstone (KVL) model [9]: KVL model is also well known as the "Tiwari and Das Model". Although the mixture of nanoparticles and base liquid is a multi-phase problem due to the existence of nanoparticles, it is assumed that the nanoparticles can be easily fluidized and as a result, the nanoliquid can almost be considered as a conventional single-phase (homogenous) fluid with average physical properties of individual phases. Furthermore, in this model, it is considered that both the liquid and particle phases are in thermal equilibrium and move with the same velocity.

2. Buongiorno model (BM) [10]: In 2006, Buongiorno conducted an extensive study of convective transport in nanoliquids and explained how and why heat transfer enhancement is observed during convective situations. He considered seven slip mechanisms namely inertia, Brownian diffusion, thermophoresis, diffusophoresis, magnus effects, liquid drainage, and gravity in the study. He studied each one of these and concluded that in the absence of turbulent effects, Brownian diffusion and thermophoresis would dominate. Based on these two effects, he derived the

conservation equations; and then onwards this model is known as the "Buongiorno nanofluid model".

3. Modified Buongiorno model (MBM): Modified Buongiorno model includes the effecti -ve properties of nanofluids along with the Brownian diffusion and thermophoresis mechanisms.

Even though nanofluids have a lot of potentials to meet the growing thirst for thermal efficiency, still scientists are eagerly looking for different varieties of fluids. Hybrid nanofluids are an advanced type of nanofluids, which exhibit a remarkable thermal efficiency as compared to nanofluids. These fluids came into existence by dispersing two or more kinds of tiny particles within the base fluid or composite nanostructures in a base fluid. This implies a homogeneous mixture possessing physicochemical properties of various substances that can hardly be imagined to exist in an individual substance. Based on nanocomposite the hybrid materials are classified into three type's namely Ceramic nano compounds ($TiO_2/Al_2O_3$, $SiO_2/Al_2O_3$, $Fe_3O_4/CNT$, $SiO_2/Ni$, $Al_2O_3/SiC$, etc.), metal nano mixtures ($Al_2O_3/Ni$, $Mg/CNT$, $MgO/Fe$, $Al_2O_3/Cu$, etc.) and Polymer nanocomposites (CNT/polymer, polymer/hydroxides, polyester/$TiO_2$, etc.). Hybrid nan- -ofluids play an active role in a wide range of heat transfer applications such as electronic cooling, automobile radiators, generator cooling, nuclear system cooling, the coolant in machining, lubrication, welding, solar heating, thermal storage, heating and cooling in buildings, biomedical, drug reduction, refrigeration and defines, etc. At the industrial level, there are positive features like chemical stability and high thermal efficiency, which enables them to perform efficiently as compared to nanofluids. The rate of heat transfer influenced by $H_2O$-based $Al_2O_3 - Cu$ hybrid nanofluid was examined by Suresh et al. [11]. The magnetohydrodynamic (MHD) flow of $Al_2O_3 - Cu$/water hybrid nanofluid over a permeable expanding plate along with suction was theoretically studied by Devi and Devi [12]. Their results showed that the hybrid nanofluid possesses higher thermal performance than mono nanoliquid. The effects of Hall current in the transport of hybrid nanoliquid past a rotating plate under nonlinear Boussinesq approximation were analyzed by Amala and Mahanthesh [13]. Nadeem et al. [14] studied the stagnation-point flow in the presence/absence of thermal slip effect by using hybrid nanofluid over a circular cylinder and they reported that the significant amount of heat transfer at the saddle and nodal points can be achieved by accounting hybrid nanofluid. The magnetohydrodynamic flow of hybrid nanoparticles ($MoS_2 - Ag$) dispersed in hybrid base fluid ($C_2H_6O_2 - H_2O$) with a statistical approach was initiated by Mahanthesh [15]. This study proved that the inclusion of nanoparticles reduces the velocity profile for assisting flow.

An annulus (the Latin word for "little ring"is an annulus, with plural annuli) is a ring-shaped object, a region bounded by two concentric circles. The adjectival form of the annulus is annular. Transport processes in annulus systems containing fluid/porous layer have been attracting the attention of researchers in the last several decades, due

to its wide range of applications such as thermal energy storage, geothermal energy utilization, petroleum reservoirs, storage of grain, buried electrical cables, etc. The fundamental nature and the growing volume of work in this area are documented in the books by Nield and Bejan [16], Ingham and Pop [17]. Natural convection between coaxial vertical cylinders partially filled with porous material was studied by Paul and Singh [18]. Basant et al. [19] analyzed the transient flow by accounting the sudden application of azimuthal pressure gradient in an annulus. Shakiba and Rahimi [20] studied the MHD mixed convective flow of nanofluid along with Brownian motion in a vertical annulus. The significance of the magnetic field on the mixed convective flow of heat generating/absorbing fluid in an annular micro-channel by considering velocity slip and temperature jump conditions was examined by Jha et al. [21]. Their results showed that the skin friction coefficient and fluid velocity have a decreasing tendency with an increase in Hartmann number. The heat transport in a vertical annulus filled with magnetized nanoparticles was inspected by Mebarek-Oudina et al. [22]. Their findings showed that the heat transport rate reduces as the length of the heater (annulus) increases.

The response surface method (RSM) is a combined mathematical and statistical technique that has been used to determine a mathematical representation between factors and responses, and to identify the cause of factors that affecting a response. The main goal of this procedure is to optimize the dependent variable (response) which is influenced by several independent variables. This approach designs the test matrix considering the number of variables (actual parameters chosen) as well as the maximum and minimum limits specified for each variable (see Box and Wilson [23]). Dehlert, Central Composite, and Box-Behnken are the three main methods of designing the response surface. Of these three methods, the basic composite design is the most reliable (see Myers et al. [24]). The main advantage of using RSM in designing experiments resulted in fewer tests and less time-consuming. Additionally, sensitivity analysis is an important key concept in computational and simulation models. It is used for different purposes on different problems. Since several variables influence the functionality of thermal systems, they have to be classified based on their degree of influence. In most cases sensitivity analysis is performed to have the essential knowledge about the data, identifying the optimum condition, interrelations of variables, and rank the variables based on their least and most dominance on the response(s). Besides, this statistical study helps designers to identify the insignificant variables and the mutual impact of variables that are most important to practical applications to improve the efficiency of the device or machine. The sensitivity analysis for the forced convective flow of nanoliquid inside a wavy channel was performed by Akbarzadeh et al. [25]. Their findings showed that the pressure drop is more dominated by channel aspect ratio compare to nanoparticle suspension and Reynolds number. The heat transfer process of a nanofluid in a solar heat exchanger was analyzed by using Response surface methodology and sensitivity analysis by Mamourian et al [26].

Pordanjani et al. [27] used the RSM for MHD nanoliquid flow inside a square enclosure and they concluded that the rate of heat transfer is reasonably affected by the magnetic strength. Vahedi et al. [28] used the RSM for magneto-nanoliquid flow over a wedge and they concluded that the heat transfer, which is reasonably affected by the change in the wedge angle. Recently, Mahanthesh and Mackolil [29] examined the significance of quadratic convection and quadratic radiation mechanisms on the nanoliquid flow over a vertical plate through sensitivity analysis and RSM.

# 2 NEED FOR THE STUDY

The usage of solar energy in India has been increased over the year due to its various applications. The efficiency of solar energy can be increased by improving the solar thermal system, which can be achieved by increasing the heat transfer coefficient of the working fluid i.e., hybrid nanofluid. Since they possess better thermal performance than classical nanofluids. The outcome of this research work serves as a good tool for solar collector's production. Also, the results are found relevant in many industrial and technological applications. The various situations related to these application-oriented problems make the modeling of the same intricate and complex. Also, the problems are both mathematically and physically challenging. Besides, obtained results will enhance the scientific knowledge and would gain the attention of researchers.

Based on literature review and hybrid nanoliquid applications concern, very less attention is given to study the dynamics of hybrid nanoliquids in an annulus (vertical/hori -zontal/inclined) employing nonlinear Boussinesq approximation (quadratic density variati -on with respect to temperature) with different physical aspects such as thermal radiation (in linear, quadratic and nonlinear form), magnetic field, variable fluid properties (variable thermal conductivity and viscosity), individual/combined effect of temperature-dependent internal heat source/sink, non-uniform heat source/sink, exponential space-based heat source/sink, and convective boundary condition. Additionally, no attention is given to study the heat and mass transport characteristics of hybrid nanoliquid ($Cu-Al_2O_3-H_2O$) in an annulus using a modified Buongiorno model.

# 3 OBJECTIVES OF THE STUDY

The main objectives of this research work is to investigate:

- The heat and mass transport of hybrid nanofluids in an annulus.
- The effectiveness of nanoparticles size, particle agglomeration, Brownian motion and thermophoresis on the hybrid nanofluids.

- The significance of nonlinear convection and nonlinear radiation effects on hybrid nanofluids.
- The individual/combined effect of temperature dependent internal heat source/sink, non-uniform heat source/sink and exponential space based heat source/sink on hybrid nanofluids.
- Statistical analysis along with parametric study.

# 4 METHODOLOGY, RESULTS: OVERVIEW OF THE RESEARCH WORK CARRIED OUT

## 4.1 PROBLEM 1: Nonlinear convective flow of hybrid nanofluid in an annulus with linearized thermal radiation

The physical configuration of the problem consists of two infinite vertical annuli, with an inner and outer radius of a and b units respectively. The quadratic convective flow of hybrid nanoliquid ($Cu - Al_2O_3 - H_2O$) with thermal radiation is considered in a vertical annulus. In addition, the suction/injection and radial magnetic field aspects are taken into account (see Fig. 1). The flow is assumed to be laminar, non-transient and unidirectional. A cylindrical coordinate system is considered in such a way that $z$-coordinate is opposite to the gravity and the radial coordinate is perpendicular to the vertical annulus. The inner and outer annulus are maintained at constant temperatures $T_1$ and $T_0$ respectively (with $T_1 > T_0$). The internal and external annuli move with a constant velocity of $Au_0$ and $Bu_0$ respectively.The following assumptions are adopted in the study: i) The base liquid and composite nanoparticles are in the thermal equilibrium state. ii) The slip velocity between the nanoparticles and base liquid is neglected. iii) All the fluid properties like density, thermal conductivity, electrical conductivity, specific heat, thermal expansion coefficient are taken as a function of nanoparticle volume fractions. iv) The nonlinear Boussinesq approximation is adopted. v) The magnetic Reynolds number is assumed to be smaller than unity($M_{Re} \ll 1$) so that the induced magnetic field is negligible in comparison with the applied magnetic field. vi) The viscous dissipation term in the energy equation is ignored as the rate of deformation is very minute. vii) The electric field is neglected due to the absence of applied voltage.

The governing equations of continuity, momentum, and energy for an incompressible hybrid nanoliquid are given below:

$$\nabla \cdot \mathbf{U} = 0, \tag{1}$$

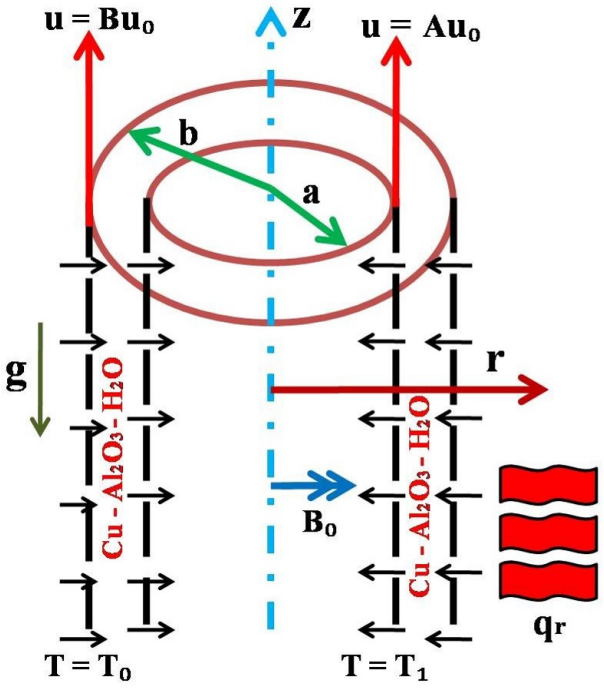


Figure 1: Physical arrangement of the problem.

$$\rho_{hnl}\left(\frac{\partial \mathbf{U}}{\partial t}+(\mathbf{U}\cdot\nabla)\mathbf{U}\right)=-\nabla p+\mu_{hnl}\nabla^2\mathbf{U}-\rho g+\mathbf{J}\times\mathbf{B_0}, \tag{2}$$

$$(\rho C_p)_{hnl}\left(\frac{\partial T}{\partial t}+(\mathbf{U}\cdot\nabla)T\right)=-\nabla(\mathbf{q}+q_r), \tag{3}$$

On adopting generalized Ohm's law the expression for current density $(J)$ is given by:

$$\mathbf{J}=\sigma_{hnl}(\mathbf{E}+\mathbf{U}\times\mathbf{B_0}), \tag{4}$$

where $\mathbf{E}=0$ since the external electric field is not applied, $\nabla=\frac{1}{r}\frac{\partial}{\partial r}\hat{r}+\frac{\partial}{\partial z}\hat{z}$ and $\mathbf{q}$ is the surface heat flux and it is given by:

$$\mathbf{q}=-k_{hnl}\nabla T, \tag{5}$$

Using Rosseland approximation the thermal radiation along the normal direction is given by:

$$q_r=\frac{-4\sigma^*}{3k^*}\left(\frac{\partial T^4}{\partial r}\right), \tag{6}$$

here, $\sigma^*$ and $k^*$ is Stefan-Boltzmann constant, and mean absorption coefficient correspondingly.

The component forms of Eqs. (1)-(3) for the steady flow in two dimensional are given

by:

$$\frac{1}{r}\frac{\partial(ru_r)}{\partial r}+\frac{\partial u_z}{\partial z}=0, \tag{7}$$

$$\begin{aligned}\rho_{hnl}\left[u_r\frac{\partial u_z}{\partial r}+u_z\frac{\partial u_z}{\partial z}\right]=&-\frac{\partial p}{\partial z}-g\rho_{hnl}-\sigma_{hnl}B_0^2u_z\\&+\mu_{hnl}\left[\frac{1}{r}\frac{\partial}{\partial r}\left(r\frac{\partial u_z}{\partial r}\right)+\frac{\partial^2u_z}{\partial z^2}\right],\end{aligned} \tag{8}$$

$$\begin{aligned}(\rho C_p)_{hnl}\left[u_r\frac{\partial T}{\partial r}+u_z\frac{\partial T}{\partial z}\right]=&k_{hnl}\left[\frac{1}{r}\frac{\partial}{\partial r}\left(r\frac{\partial T}{\partial r}\right)+\frac{\partial^2T}{\partial z^2}\right]\\&+\frac{1}{r}\frac{\partial}{\partial r}\left(r\frac{4\sigma^*}{3k^*}\frac{\partial T^4}{\partial r}\right),\end{aligned} \tag{9}$$

Since the length of the annulus is infinite, all the flow variables are assumed to be a function of $r$ alone except for the pressure gradient which is a function of $z$, then Eqs. (7)-(9) yield:

$$\frac{1}{r}\frac{d(ru_r)}{dr}=0, \tag{10}$$

$$\begin{aligned}\rho_{hnl}\left(u_r\frac{du_z}{dr}\right)=&-\frac{dp}{dz}-\sigma_{hnl}B_0^2u_z+g[(\rho\beta_0)_{hnl}(T-T_0)+(\rho\beta_1)_{hnl}(T-T_0)^2]\\&+\mu_{hnl}\left(\frac{1}{r}\frac{d}{dr}\left(r\frac{u_z}{dr}\right)\right),\end{aligned} \tag{11}$$

$$(\rho C_p)_{hnl}\left(u_r\frac{dT}{dr}\right)=\left[k_{hnl}+\frac{16\sigma^*T_0^3}{3k^*}\right]\frac{1}{r}\frac{d}{dr}\left(r\frac{dT}{dr}\right), \tag{12}$$

**The corresponding boundary conditions of the problem are:**

$$T(a)=T_1,\ u_z(a)=Au_0,\ T(b)=T_0,\ u_z(b)=Bu_0. \tag{13}$$

The velocity along radial direction can be obtained by solving Eq. (10) and it is of the form:

$$u_r=-\frac{au_{r0}}{r}. \tag{14}$$

where $u_r=-\dfrac{au_{r_0}}{r_0}$ and $u_r=-u_{r_0}$ corresponds to the rate of suction/injection at the outer and inner annulus respectively.

Introducing the following thermophysical properties for hybrid nanoliquid and the dimensi-
-onless quantities:

$$\rho_{hnl} = (1-\phi)\rho_l + (\phi\rho)_{Cu} + (\phi\rho)_{Al_2O_3},$$
$$(\rho C_p)_{hnl} = (1-\phi)(\rho C_p)_l + \phi_{Cu}(\rho C_p)_{Cu} + \phi_{Al_2O_3}(\rho C_p)_{Al_2O_3},$$
$$(\rho\beta_0)_{hnl} = (1-\phi)(\rho\beta_0)_l + \phi_{Cu}(\rho\beta_0)_{Cu} + \phi_{Al_2O_3}(\rho\beta_0)_{Al_2O_3},$$
$$(\rho\beta_1)_{hnl} = (1-\phi)(\rho\beta_1)_l + \phi_{Cu}(\rho\beta_1)_{Cu} + \phi_{Al_2O_3}(\rho\beta_1)_{Al_2O_3},$$
$$\sigma_{hnl} = \sigma_l \left[1 + \frac{3(\sigma_{Cu}-1)\phi_{Cu}}{\sigma_{Cu}+2-(\sigma_{Cu}-1)\phi_{Cu}}\right]\left[1 + \frac{3(\sigma_{Al_2O_3}-1)\phi_{Al_2O_3}}{\sigma_{Al_2O_3}+2-(\sigma_{Al_2O_3}-1)\phi_{Al_2O_3}}\right],$$

$$R = \frac{r}{a}, \quad \lambda = \frac{b}{a}, \quad \theta = \frac{T-T_0}{T_1-T_0}, \quad Z = \frac{z}{ReD_h}, \quad U = \frac{u_z}{u_0}, \quad P = \frac{p}{\rho_l u_0^2}, \quad D_h = 2(b-a). \tag{15}$$

into the Eqs. (11))-(13) then one can get:

$$a_1\frac{d^2U}{dR^2} + \frac{(1+a_1)}{R}\frac{dU}{dR} - a_3\frac{U}{R^2} - a_2 + a_4\theta + a_5\theta^2 = 0, \tag{16}$$

$$(a_6+a_7)\frac{d^2\theta}{dR^2} + \frac{(1+a_6+a_7)}{R}\frac{d\theta}{dR} = 0, \tag{17}$$

$$\theta(1) = 1, \quad U(1) = A, \quad \theta(\lambda) = 0, \quad U(\lambda) = B. \tag{18}$$

on solving Eqs. (16) and (17) using boundary conditions (18), the expression for velocity and temperature can be obtained as:

$$U(R) = C_3R^{a_9} + C_4R^{a_{10}} + t_1R^2 - t_2R^{2+a_8} - t_3R^{2(1+a_8)}, \tag{19}$$

$$\theta(R) = C_1 + C_2R^{a_8}. \tag{20}$$

The dimensionless bulk temperature can be defined as

$$\theta_b = \frac{T_b-T_0}{T_1-T_0} = \frac{\int_1^\lambda RU(R)\theta(R)dR}{\int_1^\lambda RU(R)dR} = C_1 + \frac{C_2a_{11}}{a_{12}}. \tag{21}$$

The expressions for dimensionless skin friction coefficient and Nusselt number at $R = 1$

and $R = \lambda$ are given by:

$$\tau_1 = \frac{\mu_{hnl}}{\mu_l}\left(\frac{dU}{dR}\right)_{R=1} = \frac{\mu_{hnl}}{\mu_l}[C_3 a_9 + C_4 a_{10} + 2t_1 - t_2(2+a_8) - 2t_3(1+a_8)],$$

$$\begin{aligned}\tau_\lambda = \frac{\mu_{hnl}}{\mu_l}\left(\frac{dU}{dR}\right)_{R=\lambda} &= \frac{\mu_{hnl}}{\mu_l}[C_3 a_9 \lambda^{a_9-1} + C_4 a_{10}\lambda^{a_{10}-1} + 2t_1\lambda - t_2(2+a_8)\lambda^{a_8+1} \\ &\quad - 2t_3(1+a_8)\lambda^{2a_8+1}].\end{aligned} \tag{22}$$

$$Nu_1 = -\frac{2(\lambda-1)k_{hnl}}{(\theta_{R=1}-\theta_b)k_l}\left(\frac{d\theta}{dR}\right)_{R=1} = -\frac{k_{hnl}2(\lambda-1)C_2 a_8}{(1-\theta_b)k_l},$$

$$Nu_\lambda = \frac{2(\lambda-1)k_{hnl}}{(\theta_{R=\lambda}-\theta_b)k_l}\left(\frac{d\theta}{dR}\right)_{R=\lambda} = -\frac{k_{hnl}2(\lambda-1)C_2 a_8\lambda^{a_8-1}}{\theta_b k_l}. \tag{23}$$

The analytical solutions are satisfying the imposed boundary conditions; this indicates the correctness of the solution. Further to demonstrate the accuracy of the solutions, a direct comparison is made between the analytical results and the results obtained by the Runge-Kutta-Fehlberg $4-5^{th}$ order method (RKFM) for $Nu_0$ and $Nu_\lambda$. These comparison values are in good agreement.

**where**, $a$ is the radius of inner cylinder, $b$ is the radius of outer cylinder, $A$ is the coefficient of velocity for the inner cylinder, $B$ is the coefficient of velocity for the outer cylinder, $B_0$ is the magnetic field along radial direction, $p$ is the pressure, $u_z$ is the velocity along $z$ direction , $u_r$ is the velocity in $r$ direction, $T$ is the temperature, $C_p$ is the specific heat, $k$ is the hermal conductivity, $\beta_0$&$\beta_1$ is the thermal expansion coefficients, $\mu$ is the dynamic viscosity, $\rho$ is the density, the subscripts $hnl$ and $l$ represents the hybrid nanoliquid and base liquid respectively.

### 4.1.1 Parametric Analysis

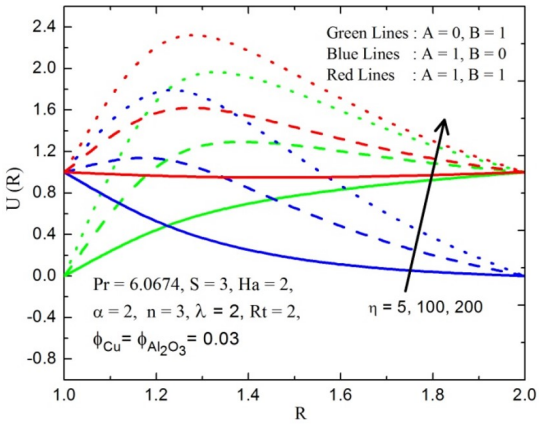


Figure 2: The variation of $\eta$ on $U(R)$.

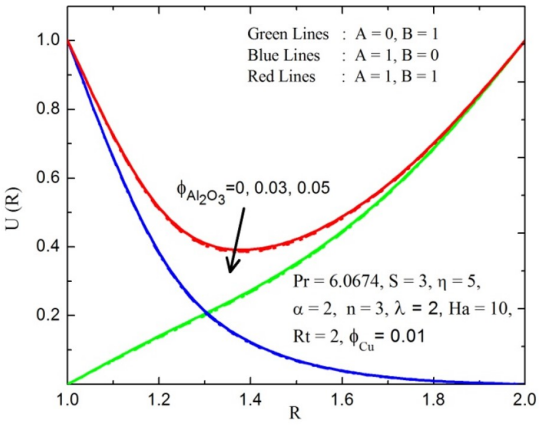


Figure 3: The variation of $\phi_{Al_2O_3}$ on $U(R)$.

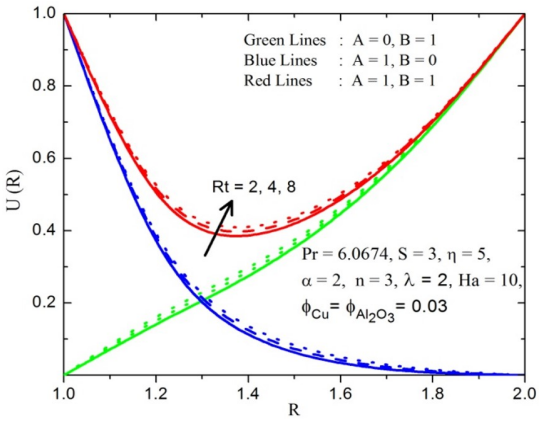


Figure 4: The variation of $Rt$ on $U(R)$.

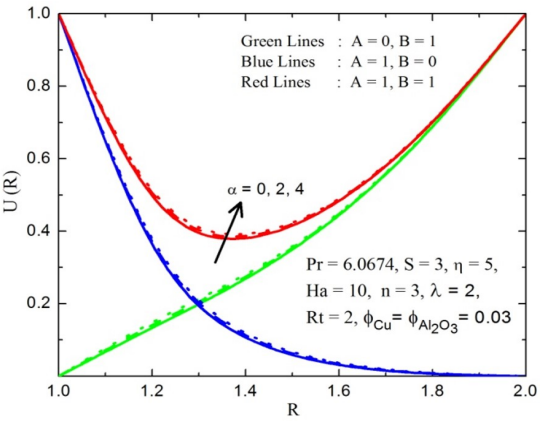


Figure 5: The variation of $\alpha$ on $U(R)$.

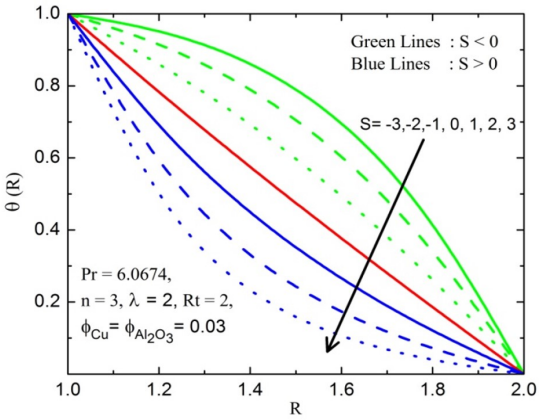


Figure 6: The variation of $S$ on $\theta(R)$.

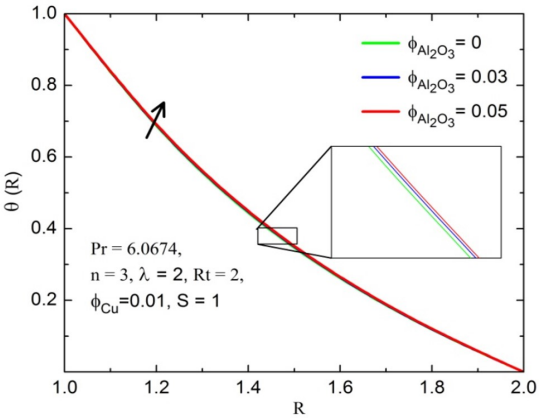


Figure 7: The variation of $\phi_{Al_2O_3}$ on $\theta(R)$.

### 4.1.2 Statistical Analysis

The statistical analysis is conducted for further analysis and it plays a significant role in computational and simulation models. Understanding the relationship between the effective parameters (independent variables) and response variables (skin friction coefficient ($\tau$) & Nusselt number ($Nu$)) is absolutely necessary. Hence, in this section statistical tools like correlation, probable error and a multivariate regression model are utilized to establish the relationship between the effective parameters and different flow fields ($\tau$ & $Nu$).

**Correlation coefficient and probable error (Cr & PE)**

The coefficient of correlation is a statistical technique which represents the strength of the connection between the pair of variables. The correlation coefficient can be positive or negative and it is represented by $Cr$ where $Cr \in [-1, 1]$. If an increase in one variable results in an enhancement in another variable then it is termed as positive correlation and the reverse phenomenon is termed as a negative correlation. The significance in the accuracy of the correlation coefficient can be calculated by using probable error($PE$). Mathematical expression to calculate $PE$ by using the Pearson product-moment method is given by:

$$PE = 0.6745\left(\frac{1 - Cr^2}{\sqrt{j}}\right). \tag{24}$$

where $j$ is the number of observations and the significance correlation is achieved if $\left|\frac{Cr}{PE}\right| > 6$.

**Regression analysis**

The regression analysis is performed to estimate $\tau_1$ and $Nu_1$ by using a multivariate linear regression model. Here, $\tau_1$ and $Nu_1$ is estimated from 30 random sets of values of effective parameter $S, Ha, \eta, Rt, \alpha$ chosen in the range [1, 10] and $\phi(= \phi_{Cu} + \phi_{Al_2O_3})$ in the range [0.01, 0.06]. It is found that all the physical parameters are significant as their $p$-value is less than 0.05. The estimated regression model for $\tau_1$ and $Nu_1$ is given by:

$$\tau_{1est} = -0.625S - 0.877Ha + 0.101\eta + 0.035Rt + 0.141\alpha - 22.313\phi + 4.241, \tag{25}$$

$$Nu_{1est} = 2.154S - 0.174Ha + 0.225\eta - 0.967Rt + 0.153\alpha + 41.904\phi + 4.934. \tag{26}$$

### 4.1.3 Results

The significance of nonlinear Boussinesq buoyancy force on the flow of magneto-hybrid nanoliquid in an annulus with radiative heat is studied analytically. The following

conclusions are drawn:

- The velocity profile for different values of suction/injection parameter has a point of intersection inside the annulus when both walls move with a constant velocity. This makes the velocity profile to be independent of the suction/injection parameter at that point.

- The temperature profile is higher for hybrid nanoliquid than that of mono nanoliquid followed by base fluid.

- The inclusion of composite nanoparticles enhances the temperature profile significantly.

- The maximum and minimum heat transfer is found on the walls of internal and external annuli respectively.

- The nonlinear convection parameter is favorable for the skin friction coefficient.

- The enhancement of radius ratio increases and decreases the heat transfer and skin friction coefficient respectively at the outside of the inner wall.

- The effect of radiation and thermal convection is qualitatively the same for all flow fields.

- The actual values and estimated values calculated for $\tau$ and $Nu$ from the multivariate linear regression model are superimposed.

## 4.2 PROBLEM 2: Nonlinear convective flow of hybrid nanofluid in an annulus with nonlinear thermal radiation

The flow is assumed to be laminar, incompressible, non-transient and unidirectional through an asymmetrically heated annulus of two infinite concentric annuli of inner radius a and outer radius b as depicted in Fig.10. The flow which is parallel to acceleration due to gravity is considered along $z$-coordinate, while radial coordinate is taken perpendicular to the annulus. An unequal constant temperatures $T_1$ and $T_0$ respectively kept at inner and outer surface of the annulus with $T_1 > T_0$ (The hybrid nanoliquid $(Cu-Al_2O_3-H_2O)$ is utilized and simulated via KVL model). In addition, the suction/injection, ESHS, and radial magnetic field aspects are taken into account. The internal and external annuli are moved with a constant velocity of $Au_0$ and $Bu_0$ respectively.

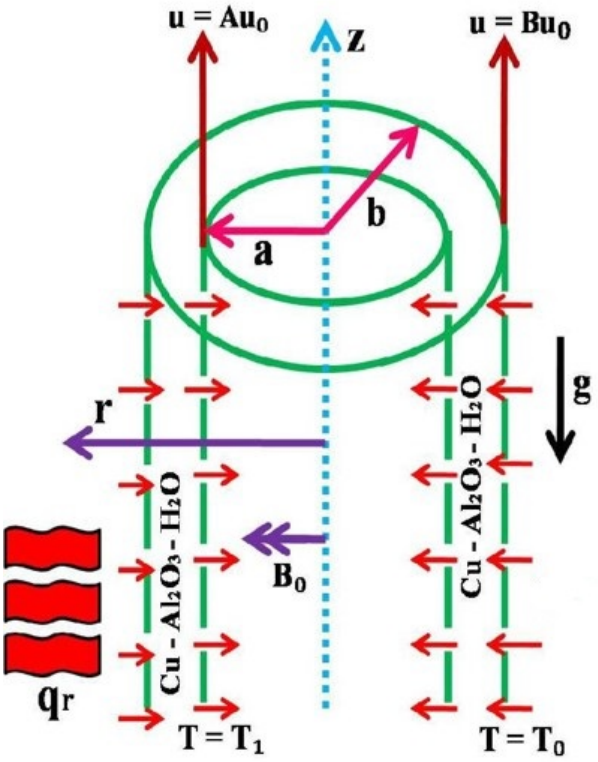


Figure 8: Flow configuration in an annulus.

**The governing equations of the problem are:**

$$\frac{1}{r}\frac{d(ru_r)}{dr} = 0, \tag{27}$$

$$\begin{aligned}\rho_{hnl}\left(u_r\frac{du_z}{dr}\right) =& -\frac{dp}{dz} - \sigma_{hnl}B_0^2u_z + g[(\rho\beta_0)_{hnl}(T-T_0) + (\rho\beta_1)_{hnl}(T-T_0)^2] \\ &+ \mu_{hnl}\left(\frac{1}{r}\frac{d}{dr}\left(r\frac{u_z}{dr}\right)\right),\end{aligned} \tag{28}$$

$$\begin{aligned}(\rho C_p)_{hnl}\left(u_r\frac{dT}{dr}\right) =& k_{hnl}\left[\frac{1}{r}\frac{d}{dr}\left(r\frac{dT}{dr}\right)\right] + \frac{1}{r}\frac{d}{dr}\left(r\frac{dT}{dr}\frac{16\sigma^*}{3k^*}T^3\right) \\ &+ (T_1-T_0)Q_e exp\left(\frac{-lr}{a}\right).\end{aligned} \tag{29}$$

**The corresponding boundary conditions of the problem are:**

$$T(a) = T_1,\ u_z(a) = Au_0,\ T(b) = T_0,\ u_z(b) = Bu_0. \tag{30}$$

Introducing thermophysical properties for hybrid nanoliquid and the dimensionless quantities

as in Eq. (15) into the Eqs. (28)-(30) then one can get:

$$\frac{d^2U}{dR^2} - \frac{1}{A_1 4(\lambda-1)^2}\left[A_2\left(\frac{dP}{dz}\right) + A_3 Ha^2\frac{U}{R^2} - \eta A_5\theta - \eta A_6\alpha\theta^2\right] + \left(\frac{SA_2}{A_1}+1\right)\frac{1}{R}\frac{dU}{dR} = 0, \tag{31}$$

$$\frac{d^2\theta}{dR^2} + \left(\frac{SA_4Pr}{A_7} + 1 + \frac{4R_T}{3A_7}(1+(\theta_w-1)\theta)^3\right)\frac{1}{R}\frac{d\theta}{dR} + \frac{4R_T}{3A_7}\left[\frac{d\theta}{dR}(1+(\theta_w-1)\theta)^3\right]' + \frac{Q_EPr}{A_7}exp(-lR) = 0, \tag{32}$$

$$\theta(1) = 1, \quad U(1) = A, \quad \theta(\lambda) = 0, \quad U(\lambda) = B. \tag{33}$$

On introducing new radiation parameter called film radiation parameter($R_f$). Which is defined as follows:

$$R_f = \frac{4\sigma^* T_f^3}{k^* k_l}, \quad \text{where} \quad T_f = \frac{T_1+T_0}{2} \quad \text{(film temperature)}. \tag{34}$$

Substituting Eq. (34) in Eq. (32) yield:

$$\frac{d^2\theta}{dR^2} + \left(\frac{SA_4Pr}{A_7} + 1 + \frac{32R_f}{3A_7(\theta_w+1)^3}(1+(\theta_w-1)\theta)^3\right)\frac{1}{R}\frac{d\theta}{dR} + \frac{Q_EPr}{A_7}exp(-lR) + \frac{32R_f}{3A_7(\theta_w+1)^3}\left[\frac{d\theta}{dR}(1+(\theta_w-1)\theta)^3\right]' = 0, \tag{35}$$

The skin friction coefficient and Nusselt number at $R = 1$ and $R = \lambda$ are given by:

$$\tau_1 = \frac{\mu_{hnl}}{\mu_l}\left(\frac{dU}{dR}\right)_{R=1}, \quad \tau_\lambda = \frac{\mu_{hnl}}{\mu_l}\left(\frac{dU}{dR}\right)_{R=\lambda}, \tag{36}$$

$$Nu_1(\theta_{R=1}-\theta_b) = -\frac{2(\lambda-1)k_{hnl}}{k_l}\left(\frac{d\theta}{dR}\right)_{R=1}, \; Nu_\lambda(\theta_{R=\lambda}-\theta_b) = \frac{2(\lambda-1)k_{hnl}}{k_l}\left(\frac{d\theta}{dR}\right)_{R=\lambda}. \tag{37}$$

Eqs. (31) and (35) subjected to the boundary condition (33) are solved by utilizing the

shooting technique. Further, a direct comparison is made between the results secured in the current study with an analytical method for temperature profile. This comparison is done by neglecting the thermal radiation and exponential heat source aspects in the energy equation.

### 4.2.1 Parametric Analysis

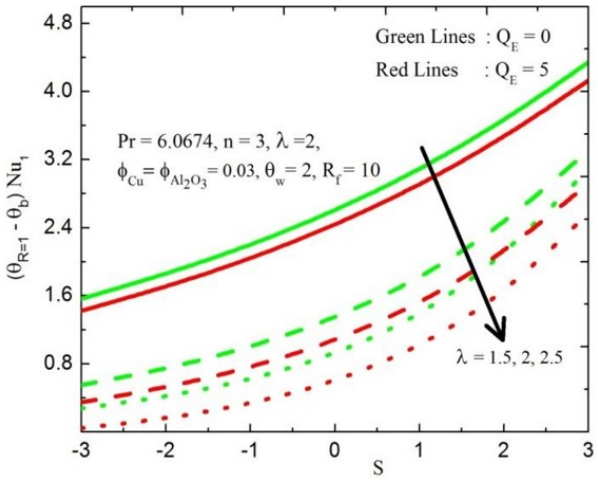


Figure 9: $(\theta_{R=1} - \theta_b)Nu_1$ for various values of $\lambda, Q_E$ and $S$.

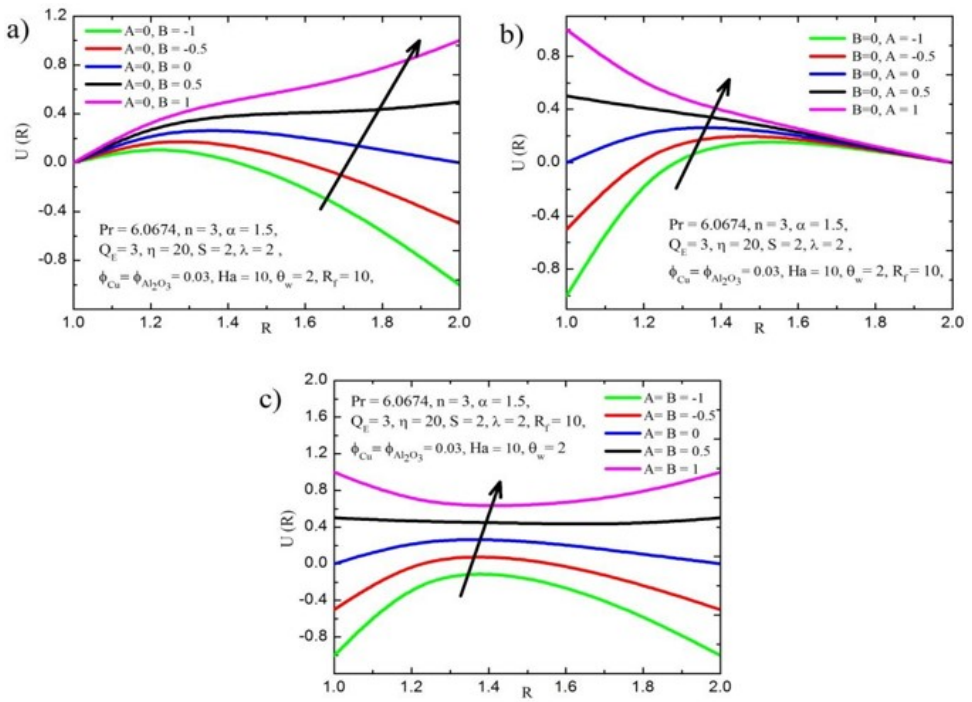
a)
A=0, B = -1
A=0, B = -0.5
A=0, B = 0
A=0, B = 0.5
A=0, B = 1
Pr = 6.0674, n = 3, α = 1.5,
$Q_E$ = 3, η = 20, S = 2, λ = 2 ,
$\phi_{Cu} = \phi_{Al_2O_3} = 0.03$, Ha = 10, $\theta_w$ = 2, $R_f$ = 10,
U (R)
R
b)
B=0, A = -1
B=0, A = -0.5
B=0, A = 0
B=0, A = 0.5
B=0, A = 1
Pr = 6.0674, n = 3, α = 1.5,
$Q_E$ = 3, η = 20, S = 2, λ = 2 ,
$\phi_{Cu} = \phi_{Al_2O_3} = 0.03$, Ha = 10, $\theta_w$ = 2, $R_f$ = 10,
U (R)
R
c)
Pr = 6.0674, n = 3, α = 1.5,
$Q_E$ = 3, η = 20, S = 2, λ = 2, $R_f$ = 10,
$\phi_{Cu} = \phi_{Al_2O_3} = 0.03$, Ha = 10, $\theta_w$ = 2
A= B = -1
A= B = -0.5
A= B = 0
A= B = 0.5
A= B = 1
U (R)
R

Figure 10: Velocity profile for various movements of annuli.

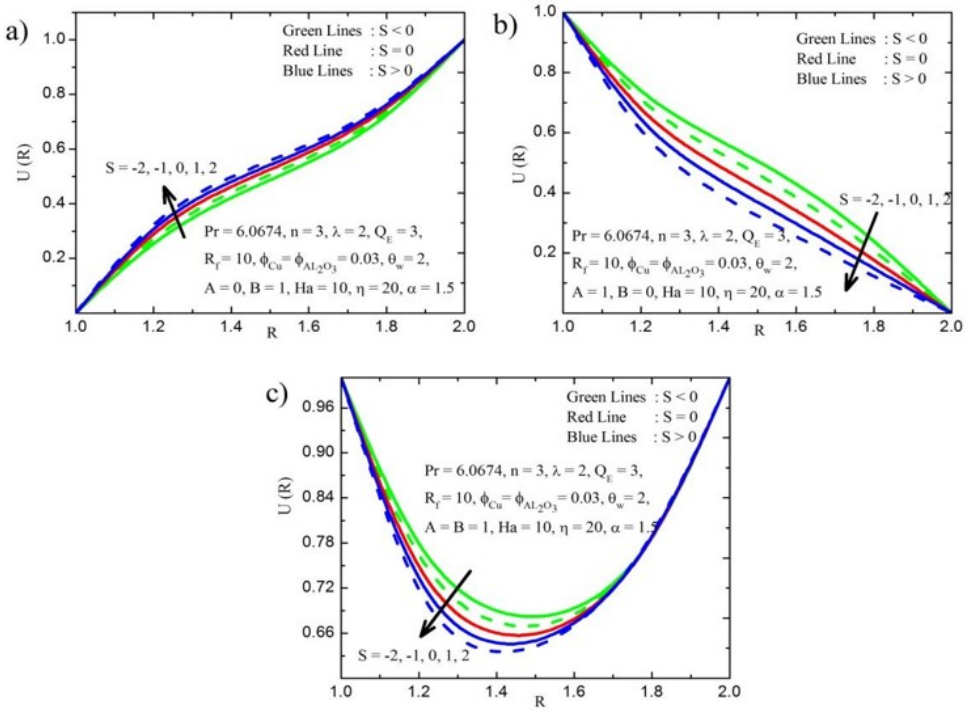


Figure 11: $U(R)$ for various values of $S$.

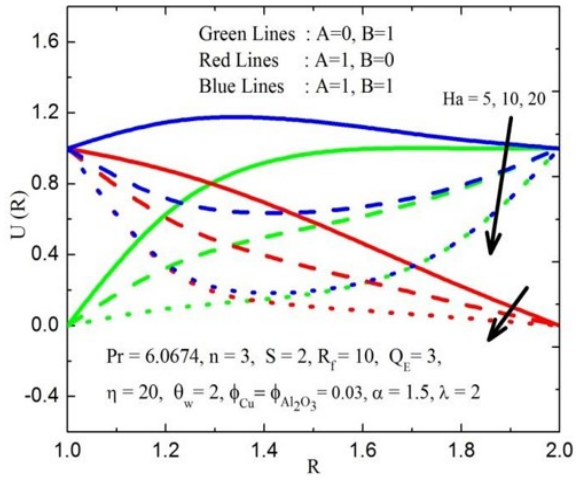


Figure 12: $U(R)$ for various values of $Ha$.

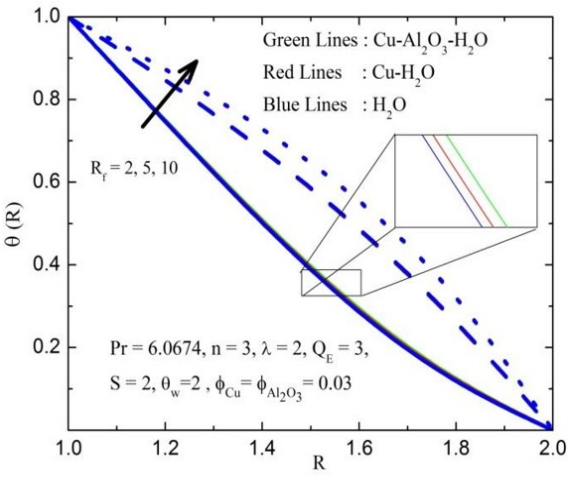


Figure 13: $\theta(R)$ for various values of $R_f$.

### 4.2.2 Statistical Analysis

**Response surface methodology (RSM)**

RSM is a hybrid mathematical-statistical approach that is useful for the approximation and optimization of stochastic models. The RSM approach not only determines the best conditions but also provides information to evaluate the results for the design of

the process. The response variables are the output results, and effective parameters are the input. A graphical representation of the response with the effective parameters is known as the response surface. Here, $\tau_1$ & $Nu_1$ are the interested response variables and $R_f, Q_E \& \phi_{Cu}$ are the chosen effective parameters. The range of effective parameters is chosen in three different levels namely low (-1), middle (0) and high (+1). A face-centered Central Composite Design (CCD) is used to fit the polynomial in the equation. The number of runs required for the experimental design is calculated by using the expression $2^f + 2f + d$, where $f$ and $d$ refer to the number of factors ($f = 3$) and the number of central points ($d = 6$) respectively. The polynomial correlation for $\tau_1$ & $Nu_1$ containing linear, square, and interaction terms of chosen effective parameters are as follows:

$$\begin{aligned}\tau_1 =& a_0 + a_1 R_f + a_2 Q_E + a_3 \phi_{Cu} + a_{12} R_f Q_E + a_{13} R_f \phi_{Cu} + a_{23} Q_E \phi_{Cu} \\ &+ a_{11} R_f^2 + a_{22} Q_E^2 + a_{33} \phi_{Cu}^2,\end{aligned} \tag{38}$$

$$\begin{aligned}Nu_1 =& b_0 + b_1 R_f + b_2 Q_E + b_3 \phi_{Cu} + b_{12} R_f Q_E + b_{13} R_f \phi_{Cu} + b_{23} Q_E \phi_{Cu} \\ &+ b_{11} R_f^2 + b_{22} Q_E^2 + b_{33} \phi_{Cu}^2.\end{aligned} \tag{39}$$

where $a_0$ & $b_0$ are the intercept, $a_i$ & $b_i$, $a_{ii}$ & $b_{ii}$ and $a_{ij}$ & $b_{ij}$ are respectively linear, square and interaction regression coefficients ($i = j = 1(1)3$).

**Accuracy of the model**

The ANOVA table composed of a statistical estimator like adjusted sum of squares, $F$-value, $p$-value, adjusted mean square, $R^2$ and adj-$R^2$ for $\tau_1$ & $Nu_1$. The ratio of mean squares is termed as $F$-value and a higher $F$-value represents the more significant effect. The $p$-value means a probability that shows the proof against the null hypothesis. However, lower the $p$-value stronger will be proof against the null hypothesis. The better model can be obtained for the higher value of $R^2$. From ANOVA table it is observed that both $\tau_1$ and $Nu_1$ models having a high coefficient of determination ($R^2 = 100\%$ and 99.99% respectively), which indicates that only 0.01% of total change cannot be explained by the model. The $F$-value for the models $\tau_1$ and $Nu_1$ are 42637.92 and 9548.38 respectively, which are significantly larger than unity. Besides, the $p$-value is accounted to check whether the terms in the models are significant or not. The terms with $p$-value $<0.05$ are significant for the model and the terms with p-value $>0.05$ are insignificant (it should be omitted). In view of this, it is noticed that the square terms of $Q_E, \phi_{Cu}$ and the interaction term $Q_E * \phi_{Cu}$ are not significant for both models as their $p$-value $>0.05$. Hence it should be removed from the models. On considering only the

significant regression coefficient, the models for $\tau_1$ and $Nu_1$ yield:

$$\begin{aligned}\tau_1 =& -3.74787 + 0.37789R_f + 0.025588Q_E - 0.212595\phi_{Cu} - 0.18529R_f^2 \\ & - 0.013002R_fQ_E - 0.002121R_f\phi_{Cu},\end{aligned} \tag{40}$$

$$\begin{aligned}Nu_1 =& 2.57483 - 1.12462R_f - 0.08310Q_E + 0.08318\phi_{Cu} + 0.67955R_f^2 \\ & + 0.05393R_fQ_E - 0.02218R_f\phi_{Cu}.\end{aligned} \tag{41}$$

Further, the accuracy of the model is examined with the help of residual plots. It is seen that the normal probability forming a straight line, which indicates that the residual distributions for both $\tau_1$ and $Nu_1$ are normal. The histogram shows that the data is approximately symmetric without much skewness. In the residuals versus fitted plot, it is clear that the maximum deviation is 0.00427 and 0.02506 respectively for $\tau_1$ and $Nu_1$. Also, in the residuals versus order plot, it is noticed that the residuals for $\tau_1$ and $Nu_1$ recoiling randomly around the zero lines. Based on these facts, it can be concluded that the chosen model has a good fit.

**Sensitivity analysis**

Sensitivity analysis is one of the most important techniques of numerical simulation which helps in determining the sensitivity of the responses($\tau_1$ & $Nu_1$) to the inputs ($R_f, Q_E \& \phi_{Cu}$) parameters. The partial derivatives of $\tau_1$ & $Nu_1$ with respect to $R_f, Q_E$ & $\phi_{Cu}$ are termed as the sensitivity of the responses to those effective input parameters. Mathematically, the partial derivatives of Eqs.(40) and (41) with respect to effective input parameters are calculated as follows:

$$\frac{\partial \tau_1}{\partial R_f} = 0.37789 - 0.37058R_f - 0.013002Q_E - 0.112121\phi_{Cu}, \tag{42}$$

$$\frac{\partial \tau_1}{\partial Q_E} = 0.025588 - 0.013002R_f, \tag{43}$$

$$\frac{\partial \tau_1}{\partial \phi_{Cu}} = -0.212595 - 0.002121R_f, \tag{44}$$

$$\frac{\partial Nu_1}{\partial R_f} = -1.12462 + 1.3591R_f + 0.05393Q_E - 0.02218\phi_{Cu}, \tag{45}$$

$$\frac{\partial Nu_1}{\partial Q_E} = -0.08310 + 0.05393R_f, \tag{46}$$

$$\frac{\partial Nu_1}{\partial \phi_{Cu}} = 0.08318 - 0.02218R_f. \tag{47}$$

Here, a positive sensitivity value implies an increase in effective input parameters causes an enhancement in the responses while a reverse nature is observed for the negative sensitivity value.

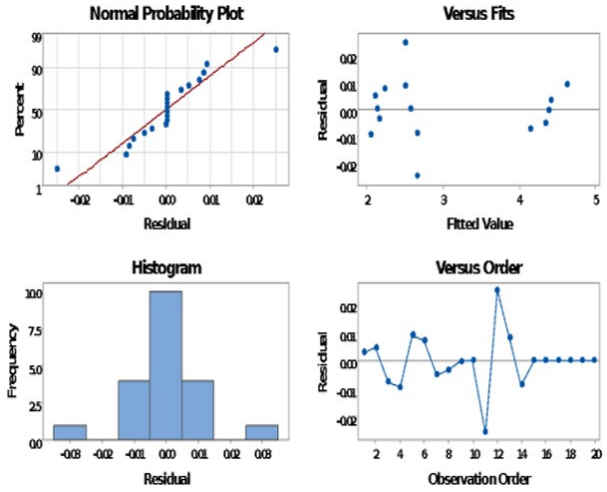


Figure 14: Residual plot for $Nu_1$.

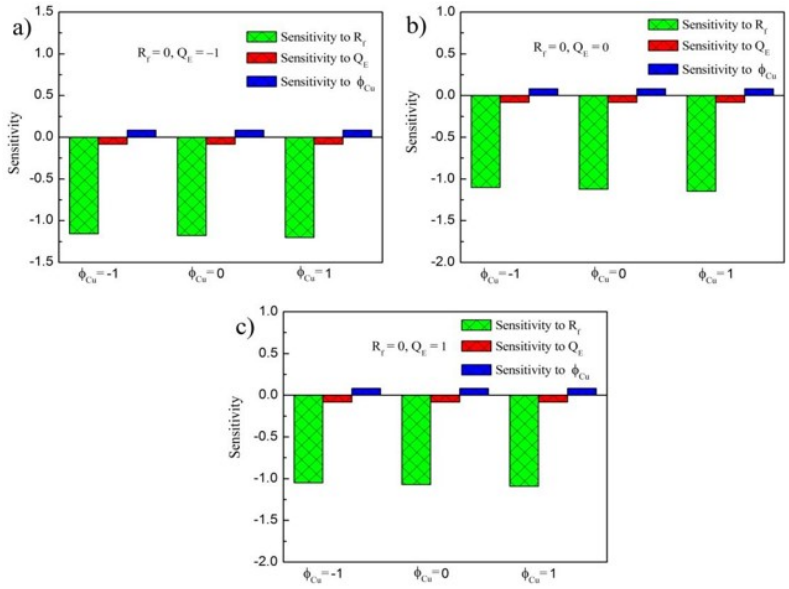


Figure 15: Sensitivity analysis for $Nu_1$ when $R_f = 0$.

### 4.2.3 Results

The nonlinear radiated heat transport of magneto-hybrid nanoliquid in an annulus subjected to nonlinear Boussinesq approximation was investigated numerically. Further, the sensitivity of responses ($\tau_1$ & $Nu_1$) to the energetic parameters such as film radiation parameter $R_f$ ($1.5 \leq R_f \leq 5.5$), exponential heat source parameter $Q_E$ ($1 \leq Q_E \leq 3$) and nanoparticle volume fraction $\phi_{Cu}$ ($0.01 \leq \phi_{Cu} \leq 0.03$) are computed by utilizing response surface methodology. Based on the results of numerical and sensitivity analysis the following conclusions are drawn

- The utilization of film radiation parameter over the classical radiation parameter leads to an asymptotic state for $\tau_1$ & $Nu_1$.
- Nonlinear thermal radiation is found to be more significant compared to linear thermal radiation for all flow fields.
- The hybrid nanoliquids have higher temperature profile than that of mono nanoliquid and followed by base liquid.
- The inclusion of nanoparticles enhances the temperature profile.
- Nonlinear convection parameter and $\phi_{Cu}$ are found to be more favorable for $\tau$ & $Nu$ respectively.
- Comparison of sensitivity depict that the skin friction coefficient is more sensitive to $R_f$ and $Q_E$ whereas Nusselt number is more sensitive to $\phi_{Cu}$.

## 4.3 PROBLEM 3: Nonlinear convective flow of hybrid nanofluid in an annulus with quadratic thermal radiation and variable fluid properties

The steady-state laminar flow of water-based hybrid nanoliquid in a micro-annulus with variable viscosity and thermal conductivity is considered. The velocity slip and temperature jump at the surface of the micro-annulus are also taken into account. The hybrid nanoliquid $Ag - MgO - H_2O$ is utilized and simulated through the KVL model. The usual cylindrical coordinates $X$ and $r$ are taken along the axis of the annuli and in the radial direction respectively (see Fig.18). The radius of the inner and outer cylinders is correspondingly taken as $r_1$ and $r_2$. The inner cylinder is maintained at the temperature $T_1$ and the outer cylinder is maintained at the temperature $T_0$, where $T_1 > T_0$. Due to the large temperature difference, the quadratic Boussinesq approximation is considered. Further to agree with this hypothesis a quadratic Rosseland approximation is accounted for optically thick media. Here, the flow depends only on $r$ coordinate due to the infinite length of the cylinders. Under these assumptions, the governing equations are given below (see Jha et al. [30], Weng [31]):

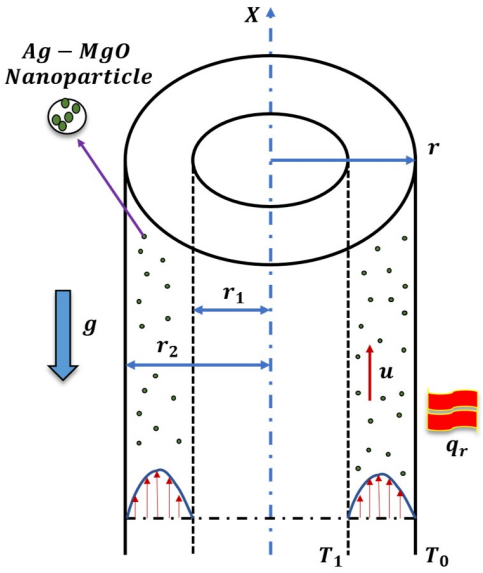


Figure 16: Physical model of the problem.

**The governing equations of the problem are:**

$$\frac{1}{r}\frac{d}{dr}\left(\mu_{hnl} r \frac{du}{dr}\right) + g[(\rho\beta_0)_{hnl}(T-T_0) + (\rho\beta_1)_{hnl}(T-T_0)^2] = 0, \tag{48}$$

$$\frac{1}{r}\frac{d}{dr}\left(k_{hnl} r \frac{dT}{dr}\right) + \frac{4\sigma^*}{3k^*}\left(\frac{4}{r}(3TT_0^2 - 2T_0^3)\frac{dT}{dr} + (12T_0^2 T - 8T_0^3)\frac{d^2T}{dr^2} + 12T_0^2\left(\frac{dT}{dr}\right)^2\right) = 0, \tag{49}$$

**Boundary conditions**

$$\begin{aligned} u &= l_1\left(\frac{du}{dr}\right)_{r=r_1}, \quad T = T_1 + l_2\left(\frac{dT}{dr}\right)_{r=r_1} \quad \text{at} \quad r = r_1 \\ u &= -l_1\left(\frac{du}{dr}\right)_{r=r_2}, \quad T = T_0 - l_2\left(\frac{dT}{dr}\right)_{r=r_2} \quad \text{at} \quad r = r_2. \end{aligned} \tag{50}$$

**The effective thermophysical properties of water-based $Ag$-$MgO$ hybrid nanoliquid**

The effective thermal expansion coefficients obtained from mixture theory are as follows (see [32]):

$$\begin{aligned} (\rho\beta_0)_{hnl} &= (1-\phi)(\rho\beta_0)_l + \phi_{Ag}(\rho\beta_0)_{Ag} + \phi_{MgO}(\rho\beta_0)_{MgO}, \\ (\rho\beta_1)_{hnl} &= (1-\phi)(\rho\beta_1)_l + \phi_{Ag}(\rho\beta_1)_{Ag} + \phi_{MgO}(\rho\beta_1)_{MgO}, \end{aligned} \tag{51}$$

The effective dynamic viscosity and thermal conductivity obtained from phenomenological

laws are as follows (see Esfe et al. [32]):

$$\begin{aligned}\mu_{hnl} &= (1 - 0.1941 \times 10^8\phi^4 + 714600\phi^3 - 7214\phi^2 + 32.795\phi)\mu_l(T),\\ k_{hnl} &= \left[\frac{\phi + 0.1747 \times 10^5}{0.1997 \times 10^8\phi^3 + 0.1117 \times 10^7\phi^2 - 0.1498 \times 10^6\phi + 0.1747 \times 10^5}\right] k_l(T).\end{aligned} \tag{52}$$

The nanoparticle volume fraction $\phi$ is taken only up to 2%. The diameter of $Ag$ and $MgO$ nanoparticles is taken as 25nm and 40nm respectively. The correlations proposed by Esfe et al. [32] are within a very good accuracy.

Here $\mu_l(T)$ is the viscosity of the base liquid and it varies inversely with temperature as follows (see Lai and Kulacki [33], Vajravelu et al. [34])

$$\frac{1}{\mu_l(T)} = \frac{1}{\mu_0}[1 + b(T - T_0)]. \tag{53}$$

The thermal conductivity $k_f(T)$ of the base liquid, varies linearly with temperature, and it is suitable for the range of (0-4000F). By following Vajravelu et al. [34] and Chiam [35], $k_f(T)$ is defined as follows:

$$k_l(T) = k_0[1 + \epsilon(T - T_0)]. \tag{54}$$

Introducing the following dimensionless quantities and effective thermophysical properties for hybrid nanoliquid in Eqs. (48)- (50), (53) and (54) (see [30], [31]):

$$\begin{aligned}&R = \frac{r - r_1}{w}, \quad w = r_2 - r_1, \quad U = \frac{u}{u_c}, \quad \theta = \frac{T - T_0}{T_1 - T_0}, \quad L_1 = \frac{l_1}{w},\\ &L_2 = \frac{l_2}{w}, \quad B_1 = b(T_1 - T_0), \quad B_2 = \epsilon(T_1 - T_0), \quad \eta = \frac{r_1}{r_2}.\end{aligned} \tag{55}$$

By the virtue of Eqs. (53) and (54), the Eqs. (48)-(50) in dimensionless form becomes:

$$\begin{aligned}&\frac{1}{(1 + B_1\theta)}\frac{d^2U}{dR^2} + \frac{1 - \eta}{[R(1 - \eta) + \eta]}\left(\frac{1}{1 + B_1\theta}\right)\frac{dU}{dR} - \frac{B_1}{(1 + B_1\theta)^2}\frac{d\theta}{dR}\frac{dU}{dR}\\ &+ \frac{A_2}{A_1}\theta + \frac{A_3Q_c\theta^2}{A_1} = 0,\end{aligned} \tag{56}$$

$$\begin{aligned}&\left(1 + B_2\theta + \frac{4R_T}{3A_4}[3(\theta_w - 1)\theta + 1]\right)\frac{d^2\theta}{dR^2} + \left(B_2 + \frac{4R_T}{A_4}(\theta_w - 1)\right)\left(\frac{d\theta}{dR}\right)^2\\ &+ \frac{1 - \eta}{[R(1 - \eta) + \eta]}\left(1 + B_2\theta + \frac{4R_T}{3A_4}[3(\theta_w - 1)\theta + 1]\right)\frac{d\theta}{dR} = 0,\end{aligned} \tag{57}$$

$$
\begin{aligned}
U(0) &= L_1 \left(\frac{dU}{dR}\right)_{R=0}, \quad \theta(0) = 1 + L_2 \left(\frac{d\theta}{dR}\right)_{R=0}, \\
U(1) &= -L_1 \left(\frac{dU}{dR}\right)_{R=1}, \quad \theta(1) = -L_2 \left(\frac{d\theta}{dR}\right)_{R=1}.
\end{aligned} \tag{58}
$$

The Nusselt number and skin friction coefficient at $R = 0$ and $R = 1$ are given below (see [30], [31]):

$$
Nu_0 = -\frac{k_{hnl}}{k_l(T)} \left(1 + \frac{4R_T}{3}(3(\theta_w - 1)\theta(0) + 1)\right) \theta'(0), \tag{59}
$$

$$
Nu_1 = -\frac{k_{hnl}}{k_l(T)} \left(1 + \frac{4R_T}{3}(3(\theta_w - 1)\theta(1) + 1)\right) \theta'(1), \tag{60}
$$

$$
\tau_0 = \frac{\mu_{hnl}}{\mu_l(T)} U'(0), \tag{61}
$$

$$
\tau_1 = -\frac{\mu_{hnl}}{\mu_l(T)} U'(1). \tag{62}
$$

The nonlinear Eqs. (56)-(58) that govern the dynamics of composite nanoliquid has been solved numerically using the finite difference method based bvp5c algorithm. The algorithm used has been validated by direct comparison. The data of the velocity as compared with Jha et al. [30] and Weng [31] for numerous values of $\eta$. A tremendous association found and offers confirmation to the validity of the present numerical solutions.

### 4.3.1 Parametric Analysis

The influence of governing parameters such as velocity slip coefficient $L_1$, temperature jump coefficient $L_2$, radius ratio $\eta$, quadratic connection $Q_c$, quadratic thermal radiation $R_T$, viscosity variation aspect $B_1$, temperature variation aspect $B_2$, temperature ratio $\theta_w$ and total nanoparticles volume fraction $\phi$ on the flow fields are visualized through 2D plots. For numerical computation, the default values for the effective parameters ($L_1 = 0.05, L_2 = 0.008, \eta = 0.5, \theta_w = 1.5, B_1 = 0.5, B_2 = 0.3, Q_c = 0.4, \phi = 2\%$, and $R_T = 2$) has been carefully selected from standard sources, namely Jha and his collaborators [30] and Weng [31].

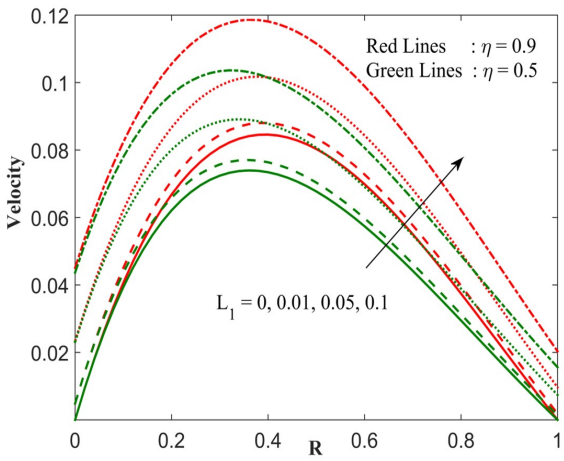


Figure 17: Velocity for various values of $L_1$ and $\eta$.

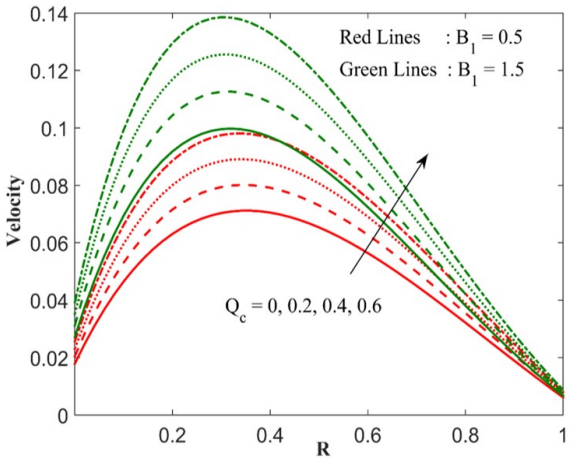


Figure 18: Velocity for various values of $Q_c$ and $B_1$.

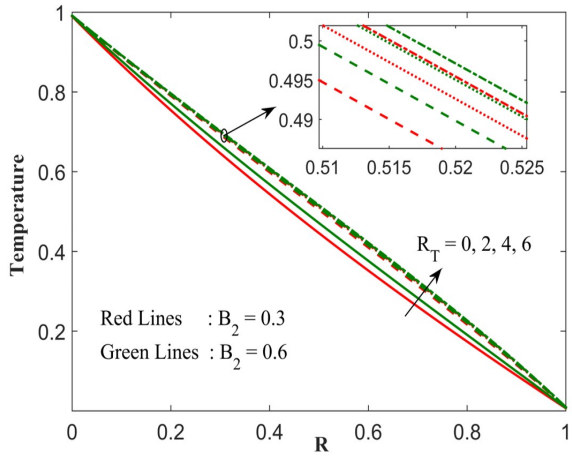


Figure 19: Temperature for various values of $R_T$ and $B_2$.

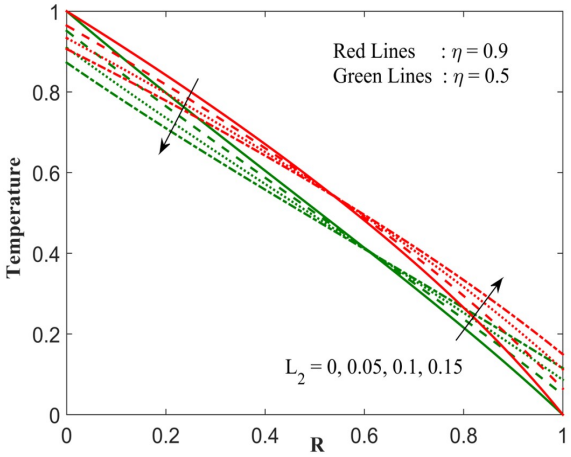


Figure 20: Temperature for various values of $L_2$ and $\eta$.

### 4.3.2 Statistical Analysis

**Response surface methodology (RSM)**

In the present study the influence of chosen input parameters $R_T, B_2$ and $\phi$ on the response variable $Nu_0$ is analyzed through RSM. The range of three input parameters at three levels is considered as $1 \leq R_T \leq 3$, $0.3 \leq B_2 \leq 0.7$ and $0.005 \leq \phi \leq 0.015$. The statistical significance and the feasibility of the developed quadratic model is verified by ANOVA table. The reduced model for $Nu_0$ by considering only the statistically significant terms from ANOVA is as follows:

$$Nu_0 = 3.59564R_T - 0.069083B_2 + 0.329095\phi - 0.00462R_T^2 - 0.01065\phi^2 + 0.136004R_T\phi - 0.004815B_2\phi + 8.56263. \tag{63}$$

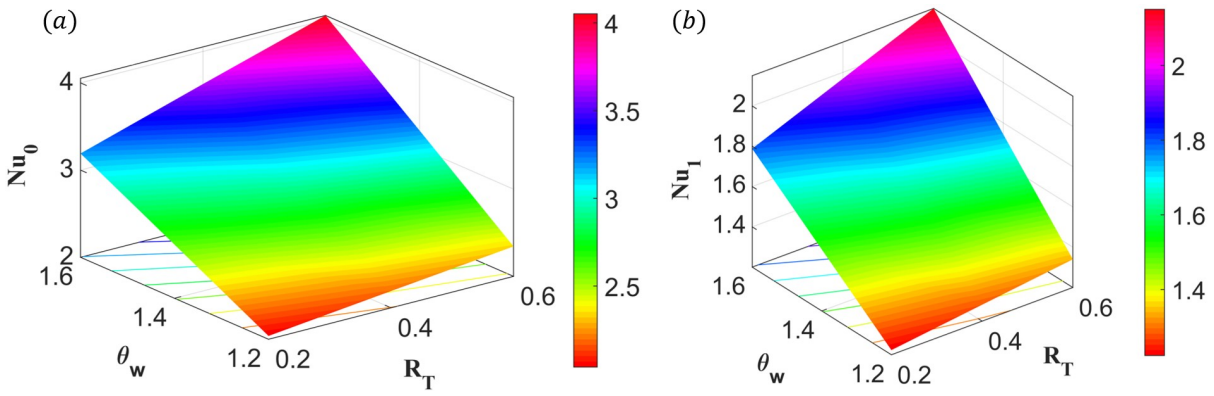


Figure 21: Nusselt number (a) $Nu_0$ and (b) $Nu_1$ for changed values of $\theta_w$ and $R_T$.

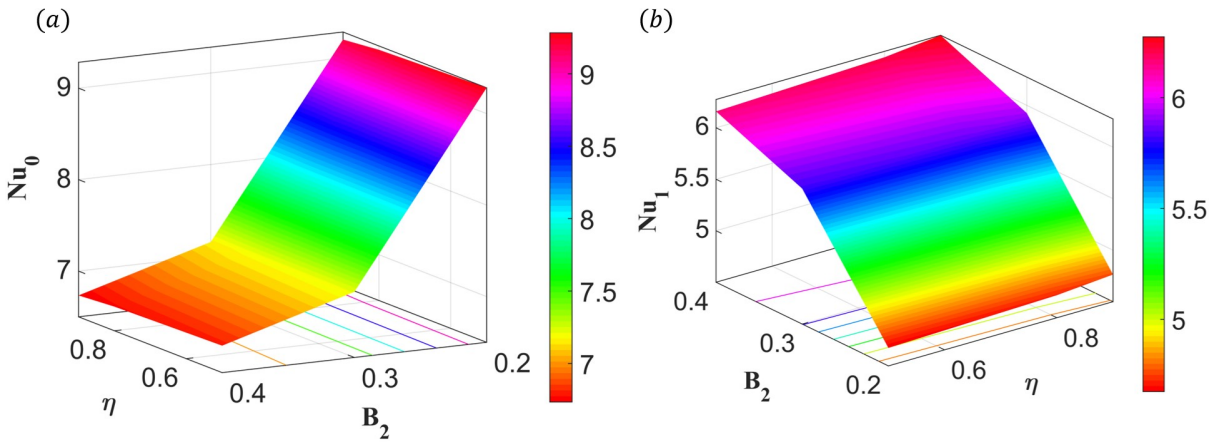


Figure 22: Nusselt number (a) $Nu_0$ and (b) $Nu_1$ for changed values of $\eta$ and $B_2$.

### Sensitivity analysis

In the current study, the sensitivity of heat transport rate $Nu_0$ to a small change in the input parameters is analyzed under specifically defined conditions. The derivative of $Nu_0$ to input parameters $R_T, B_2$ and $\phi$ define the sensitivity of heat transport rate to those effective parameters. The derivative form of Eq. (63) to effective parameters $R_T, B_2$ and $\phi$ are calculated as follows:

$$\frac{\partial Nu_0}{\partial R_T} = 3.59564 - 0.00924R_T + 0.136004\phi, \tag{64}$$

$$\frac{\partial Nu_0}{\partial B_2} = -0.069083 - 0.004815\phi, \tag{65}$$

$$\frac{Nu_0}{\partial\phi} = 0.329095 - 0.02130\phi + 0.136004R_T - 0.004815B_2. \tag{66}$$

Here, the positive and negative value of the sensitivity respectively indicates an increase and decrease in $Nu_0$ due to an enhancement in the effective parameters $R_T$,$B_2$ and $\phi$. The numerical values are obtained for $Nu_0$ with $B_2$ at the middle level (0), the quadratic radiation aspect $R_T$ and $\phi$ with levels of low (-1), middle (0), and high (+1).

### 4.3.3 Results

The main results of the current study are summarized below:

- The quadratic radiation and radius ratio lead to enhancement in the temperature and velocity profiles.
- The consequence of quadratic convection, velocity slip coefficient, and variable viscosity aspect is favorable for the velocity field.
- The velocity field declines with the addition of nanoparticles.
- The temperature field increases and decreases respectively at the inner cylinder and the outer cylinder due to the higher value of the temperature jump coefficient.
- The variable viscosity, quadratic convection, and quadratic thermal radiation mechanisms lead to higher skin friction.
- The heat transport rate improves with quadratic radiation and temperature ratio aspect.
- The rate of heat transport near the outer cylinder $Nu_1$ strengthened due to higher values of temperature variation parameter $B_2$. Whereas reverse behavior is observed near the inner cylinder.
- The heat transport is more dominated by quadratic radiation compared to the addition of nanoparticles and temperature variation aspect.
- The sensitivity of Nusselt number $Nu_0$ to the nanoparticle suspension and quadratic radiation $R_T$ is always positive.

## 4.4 PROBLEM 4: Nonlinear convective flow of hybrid nanofluid in an annulus with an induced magnetic field

Consider a non-transient, laminar flow of $Ag - MgO/H_2O$ hybrid nanoliquid in an infinite concentric annulus. The $z^{'}$- axis is defined in the vertically upward direction of annuli and $r^{'}$-axis normal to it (see Fig. 25). A magnetic field of the form $\frac{aH_0^{'}}{r^{'}}$ is applied along the radial direction. The quadratic thermal radiation and quadratic convection aspects are also taken into account. The annulus interior and exterior radius is taken as a and b correspondingly, while $T_f^{'}$ and $T_w^{'}$ represents the ambient temperature and temperature at the exterior surface of the internal cylinder respectively. The thermal equilibrium state between base liquid and composite nanoparticles is assumed. Further, the slip velocity between the base liquid and nanoparticles is neglected.

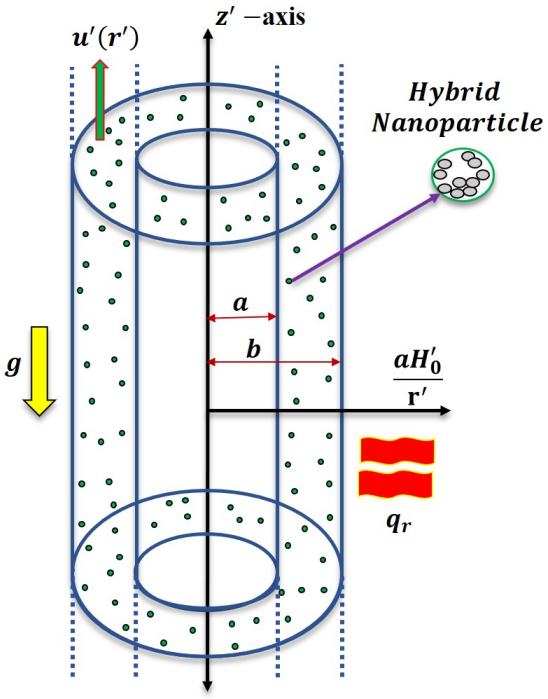


Figure 23: Model of physical problem.

**The governing equations of the problem are:**

$$\mu_{hnl}\left(\frac{d^2u^{'}}{dr^{'2}}+\frac{1}{r^{'}}\frac{du^{'}}{dr^{'}}\right)+g[(\rho\beta_0)_{hnl}(T^{'}-T_f^{'})+(\rho\beta_1)_{hnl}(T^{'}-T_f^{'})^2] + \frac{a\mu_e H_0^{'}}{r^{'}}\frac{dH_{z^{'}}^{'}}{dr^{'}}=0, \tag{67}$$

$$\eta\left(\frac{d^2H_{z'}^{'}}{dr'^2}+\frac{1}{r'}\frac{dH_{z'}^{'}}{dr'}\right)+\frac{aH_0^{'}}{r'}\frac{du'}{dr'}=0, \tag{68}$$

$$\begin{aligned}&\frac{k_{hnl}}{(\rho C_p)_{hnl}}\left(\frac{d^2T'}{dr'^2}+\frac{1}{r'}\frac{dT'}{dr'}\right)+\frac{1}{(\rho C_p)_{hnl}}\frac{1}{r'}\frac{d}{dr'}\left(r'\frac{4\sigma^*}{3k^*}[-8T_f'^3+12T'T_f'^2]\frac{dT'}{dr'}\right)\\&-\frac{k_{hnl}}{(\rho C_p)_{hnl}a^2}\left[\frac{A^*(T_w'-T_f')u'}{U}+B^*(T'-T_f')\right]=0,\end{aligned} \tag{69}$$

**The corresponding boundary conditions are (see [36],[37]):**

$$\begin{aligned}&u'=H_{z'}^{'}=0,\quad T'=T_w' \quad \text{at} \quad r'=a,\\&u'=H_{z'}^{'}=0,\quad T'=T_f' \quad \text{at} \quad r'=b.\end{aligned} \tag{70}$$

Introducing effective thermophysical properties for hybrid nanoliquid as in Eqs. (51) & (52) and succeeding dimensionless quantities (see [37]):

$$u=\frac{u'}{U},\quad r=\frac{r'}{a},\quad \lambda=\frac{b}{a},\quad T=\frac{T'-T_f'}{T_w'-T_f'}, \tag{71}$$

into the Eqs. (78)-(81) yields:

$$\frac{d^2u}{dr^2}+\frac{1}{r}\frac{du}{dr}+\frac{A_2}{A_1}T+\frac{A_3}{A_1}\alpha T^2+\frac{Ha^2}{A_1}\frac{1}{r}\frac{dH}{dr}=0, \tag{72}$$

$$\frac{d^2H}{dr^2}+\frac{1}{r}\frac{dH}{dr}+\frac{1}{r}\frac{du}{dr}=0, \tag{73}$$

$$\begin{aligned}&\left[1+\frac{4Rt}{3A_4}(1+3(\theta_w-1)T)\right]\frac{d^2T}{dr^2}+\left[1+\frac{4Rt}{3A_4}(1+3(\theta_w-1)T)\right]\frac{1}{r}\frac{dT}{dr}\\&+\frac{4Rt}{A_4}(\theta_w-1)\left(\frac{dT}{dr}\right)^2+A^*u+B^*T=0,\end{aligned} \tag{74}$$

$$\begin{aligned}&u=0,\quad H=0,\quad T=1 \quad \text{at} \quad r=1,\\&u=0,\quad H=0,\quad T=0 \quad \text{at} \quad r=\lambda.\end{aligned} \tag{75}$$

The physical quantities, skin friction coefficient ($\tau_1\&\tau_\lambda$) and Nusselt number ($Nu_1\&Nu_\lambda$)

at $r = 1$ and $r = \lambda$ are as follows (see [36], [37]):

$$\tau_1 = \frac{\mu_{hnl}}{\mu_l}\left(\frac{du}{dr}\right)_{r=1}, \qquad \tau_\lambda = -\frac{\mu_{hnl}}{\mu_l}\left(\frac{du}{dr}\right)_{r=\lambda}, \tag{76}$$

$$Nu_1 = -\frac{k_{hnl}}{k_l}\left(\frac{dT}{dr}\right)_{r=1}, \qquad Nu_\lambda = -\frac{k_{hnl}}{k_l}\left(\frac{dT}{dr}\right)_{r=\lambda}. \tag{77}$$

The $\theta$-direction induced current density is as follows (see [36], [37]):

$$J_\theta = -\frac{dH}{dr}. \tag{78}$$

Eqs. (72)-(74) accompanied by boundary conditions (75) have been solved numerically using the finite difference method implementing bvp4c. To validate the results obtained by the employed method, the values of $\tau_1$ and $\tau_\lambda$ is compared with previously published data in the absence of hybrid nanoparticles and fixing $\alpha = A^* = B^* = Rt = 0$. The comparison shows a favorable agreement.

### 4.4.1 Parametric Analysis

In this section, the impact of effective parameters on fluid flow characteristics like velocity $(u)$, induced magnetic field $(H)$, temperature $(T)$ and induced current density field $(J_\theta)$ distributions are examined graphically.The total nanoparticle volume fraction $(\phi)$ is taken only up to 2%. Also, for the numerical computation, the value for the effective parameters are taken as $\alpha = 1.5, Ha = 2, Rt = 3, \theta_w = 2, A^* = 0.1, B^* = 0.3 and \phi_{Ag} = \phi_{MgO} = 0.01$ unless otherwise specified.

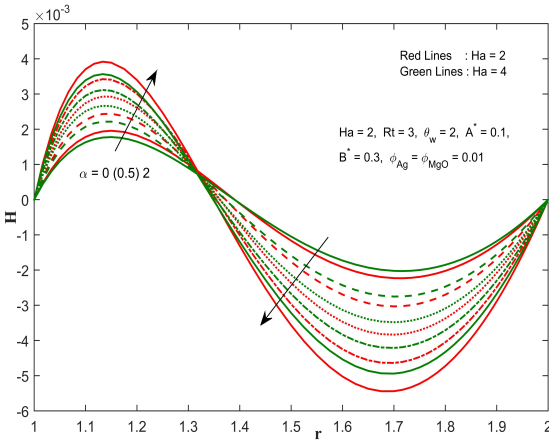


Figure 24: Impact of $Ha$ and $\alpha$ on $H$.

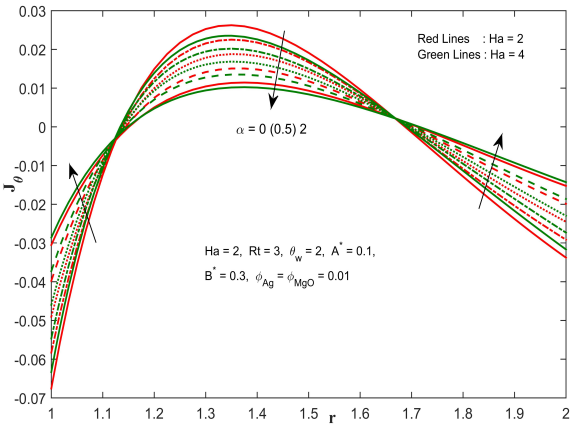


Figure 25: Impact of $Ha$ and $\alpha$ on $J_\theta$.

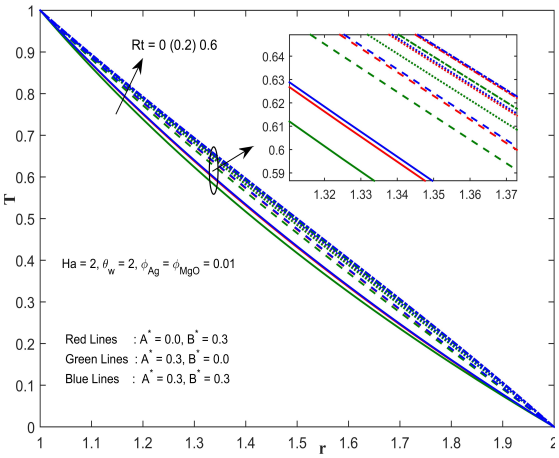


Figure 26: Impact of $A^*$,$B^*$ and $Rt$ on $T$.

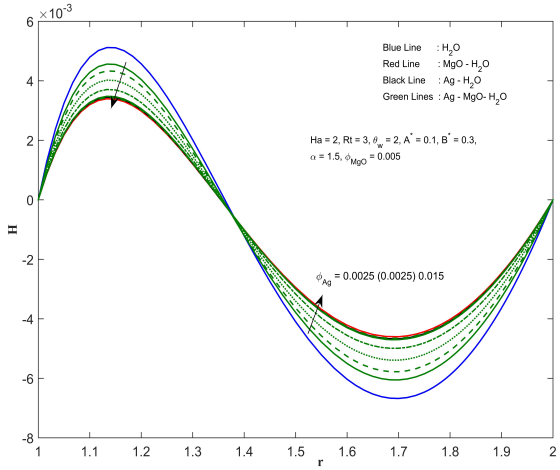
Blue Line : $H_2O$
Red Line : MgO - $H_2O$
Black Line : Ag - $H_2O$
Green Lines : Ag - MgO- $H_2O$
Ha = 2, Rt = 3, $\theta_w$ = 2, A* = 0.1, B* = 0.3,
$\alpha$ = 1.5, $\phi_{MgO}$ = 0.005
$\phi_{Ag}$ = 0.0025 (0.0025) 0.015
H
r

Figure 27: Impact of $\phi_{Ag}$ on $H$.

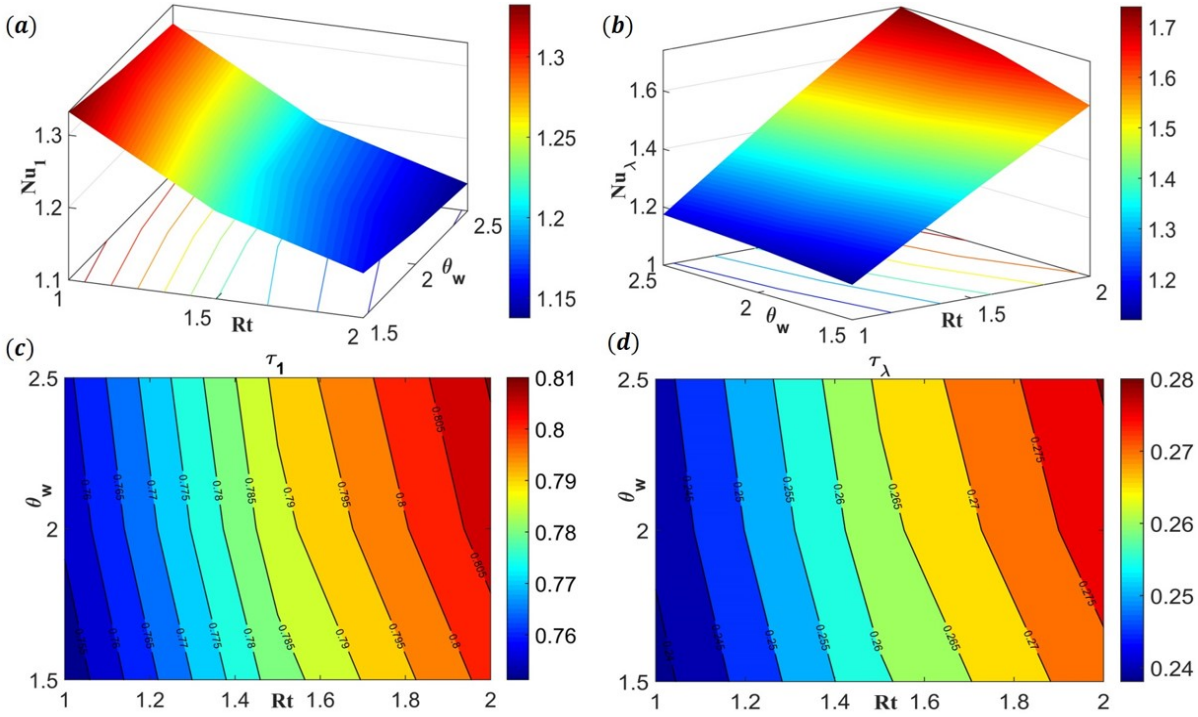


Figure 28: Impact of $Rt$ and $\theta_w$ on (a) $Nu_1$, (b) $Nu_\lambda$ (c) $\tau_1$ and (d) $\tau_\lambda$.

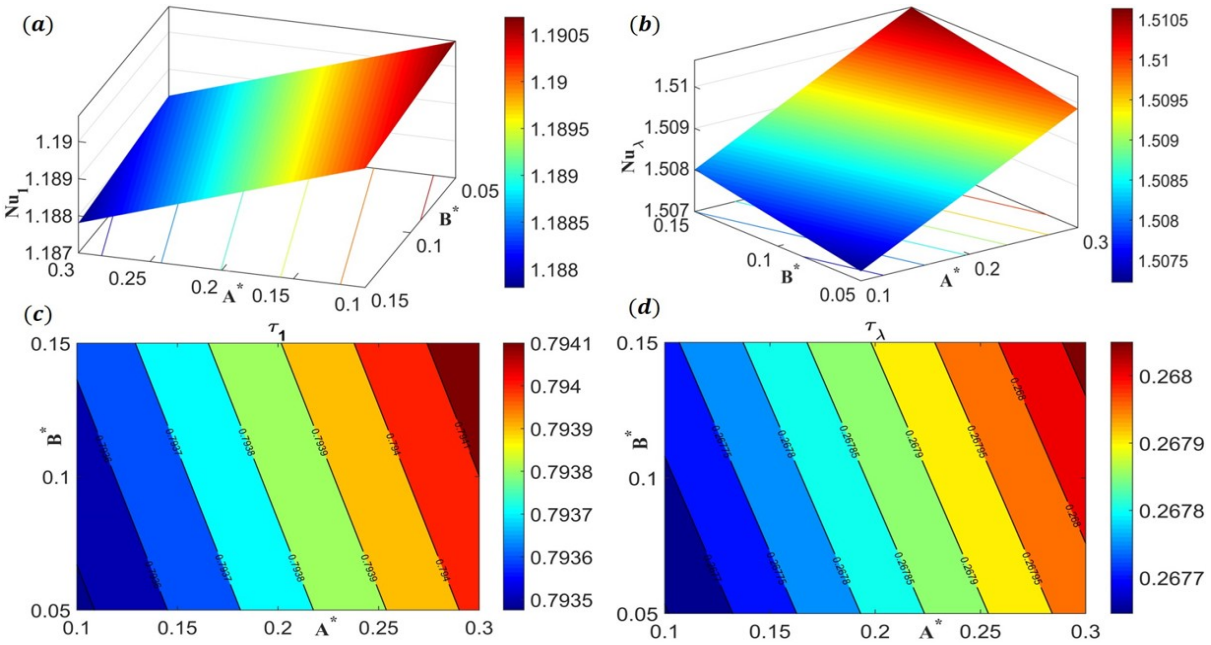


Figure 29: Impact of $A^*$ and $B^*$ on (a) $Nu_1$, (b) $Nu_\lambda$ (c) $\tau_1$ and (d) $\tau_\lambda$.

### 4.4.2 Statistical Analysis

**Response surface methodology**

The response variables are the output results, and effective parameters are the input. A graphical representation of the response with the effective parameters is known as the response surface. Here, $Nu_1$ is the interested response variable and $Rt, \alpha, A^*$ are the chosen effective parameters. The model for $Nu_1$ by considering only the statistically noteworthy regression coefficients from ANOVA yields:

$$\begin{aligned} Nu_1 = &- 0.017830Rt - 0.000134\alpha - 0.000486A^* + 0.008172Rt^2 + 0.000063Rt\alpha \\ &+ 0.000229RtA^* - 0.000070\alpha A^*. \end{aligned} \tag{79}$$

**Sensitivity analysis**

The sensitivity of $Nu_1$ towards $Rt, \alpha$ and $A^*$ were examined through CCD-RSM. The partial derivatives of $Nu_1$ with respect to $Rt, \alpha$ and $A^*$ are as follows:

$$\frac{Nu_1}{\partial Rt} = -0.017830 + 0.016344Rt + 0.000063\alpha + 0.000229A^*,$$

$$\frac{\partial Nu_1}{\partial \alpha} = -0.000134 + 0.000063Rt - 0.000070A^*, \tag{80}$$

$$\frac{\partial Nu_1}{\partial A^*} = -0.000486 + 0.000229Rt - 0.000070\alpha.$$

The sensitivity of $Nu_1$ is calculated by fixing $A^*$ at the middle level ($A = 0$).

### 4.4.3 Results

The main outcomes of this study are:

- The Hartmann number and nanoparticle volume fraction are found to be a decreasing factor for fluid velocity.
- The velocity distribution and friction factor are strengthened in the presence of non-uniform heat source/sink, quadratic convection, and quadratic thermal radiation mechanisms.
- The induced magnetic field distribution improves near the interior annulus by increasing the quadratic convection and the quadratic thermal radiation aspects.
- The Hartmann number and quadratic convection upsurge the induced current density in the domine $r \in [1, 1.1)$ and $r \in (1.65, 2]$ while in the domine $r \in (1.1, 1.65)$ the induced current density declines.
- The influence of quadratic thermal radiation and non-uniform heat source/sink upsurge the temperature profile, due to the availability of extra heat to the fluid system in the form of electromagnetic waves.
- The heat transport of composite nanoliquid for the space-related heat source/sink is observed to be higher than the temperature-related heat source/sink.
- The nanoparticle volume fraction leads to weakening the friction factor at the rate of 7.60% near the interior annulus and 8.09% near the exterior annulus.
- Due to the quadratic thermal radiation, quadratic convection, and non-uniform heat source/sink, the rate of heat transport near the exterior annulus augments at the rate of 2.98%, 0.0039%, and 0.08% respectively.
- The sensitivity of Nusselt number (at $r = 1$) towards quadratic thermal radiation, quadratic convection, and space-related heat source/sink has an inverse association.
- The quadratic thermal radiation parameter exerts a vigorous impact on the heat transport rate specifically when quadratic thermal radiation and quadratic convection are at a low level ($-1$).

## 4.5 PROBLEM 5: Nonlinear convective flow of hybrid nanofluid with temperature and space dependent internal heat sources

The mixed convective flow of water-based $Cu - Al_2O_3$ hybrid nanoliquid in an inclined porous-annulus is considered (see Fig. 32). The convective boundary conditions $k_{hnl}\dfrac{\partial T}{\partial r} = h_1(T - T_0)$ and $k_{hnl}\dfrac{\partial T}{\partial r} = -h_2(T - T_w)$ are applied respectively at the inner and outer cylinder. The usual cylindrical coordinate system with $r$-axis in the radial direction and $z$-axis as the common axis for the annulus is considered. Since the annulus of infinite length, the fluid flow is independent of $z$, hence the interested domine is defined by $r$-axis, where $a \leq r \leq b$. Here the radius of the inner and outer cylinder is correspondingly $a$ and $b$ units. The fluid is incompressible, non-transient, heat-conducting and nonlinear Boussinesq approximation is valid. The heat transport rate and flow structure are described by considering the Darcy law for the porous medium, temperature-dependent heat source (THS), and exponential space-dependent heat source (ESHS) aspects. The impact of viscous dissipation, Joule heating are not included. Of these, the governing equations for laminar flow inside the annulus using Khanafer-Vafai-Lightstone (KVL) model are as follows (following Shahzadi and Nadeem [38], Oni [39]):

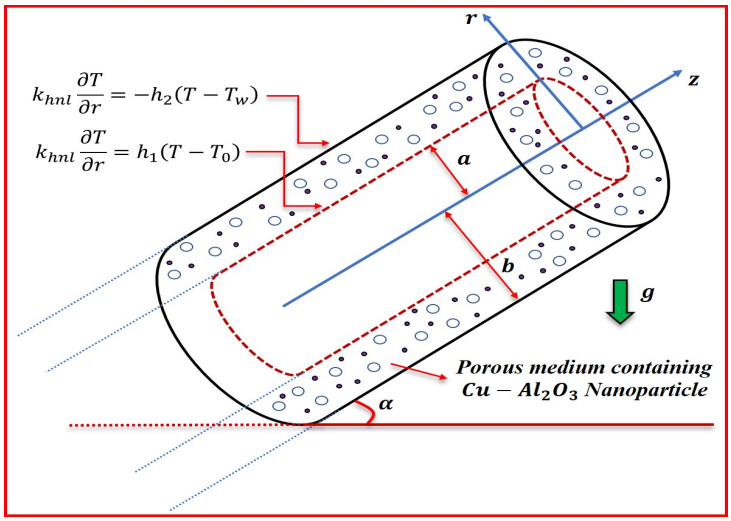


Figure 30: Physical arrangement of the problem.

**The governing equations of the problem are:**

$$\frac{\nu_{hnl}}{r}\frac{d}{dr}\left(r\frac{du^{'}}{dr}\right) + g[\beta_0(T - T_0) + \beta_{1hnl}(T - T_0)^2]cos(\alpha) - \frac{u^{'}\nu_{hnl}}{K} - \frac{1}{\rho_{hnl}}\frac{dp}{dz} = 0, \tag{81}$$

$$\frac{k_{hnl}}{(\rho C_p)_{hnl}}\left[\frac{1}{r}\frac{d}{dr}\left(r\frac{dT^{'}}{dr}\right)\right] + \frac{Q_0(T - T_0)}{(\rho C_p)_{hnl}} + \frac{(T_w - T_0)}{(\rho C_p)_{hnl}}Q_e exp\left(\frac{-nr}{a}\right) = 0, \tag{82}$$

**Subjected to the boundary conditions (see Srinivasacharya et al. [40])**

$$\begin{aligned} &\text{at} \;\; r = a: \;\; u^{'} = 0, \;\; k_{hnl}\frac{dT}{dr} = h_1(T - T_0), \\ &\text{at} \;\; r = b: \;\; u^{'} = 0, \;\; k_{hnl}\frac{dT}{dr} = -h_2(T - T_w). \end{aligned} \tag{83}$$

where $u^{'}$ denotes the velocity, $T, g, \alpha, Q_o, K, Q_e, n, \rho, k, C_p, \nu, h_1$ and $h_2$ corresponds to temperature, acceleration due to gravity, angle of inclination, THS coefficient, permeability, ESHS coefficient, exponential index, density, thermal conductivity, specific heat at constant pressure, viscosity, convective heat transport coefficient at the inner cylinder, and convective heat transport coefficient at the outer cylinder. The subscript hnl represents the hybrid nanoliquid.

Introducing the following dimensionless quantities and effective thermophysical properties for hybrid nanoliquid as in Eq. (15) (see [8]):

$$\begin{aligned} &U = \frac{u^{'}}{u_0}, \;\; P = \frac{pa}{u_0\mu_l}, \;\; Da = \frac{K}{a^2}, \\ &\theta = \frac{T - T_0}{T_w - T_0}, \;\; R = \frac{r}{a}, \;\; Z = \frac{z}{a}. \end{aligned} \tag{84}$$

Eqs. (92)-(94) become

$$A_1\left(\frac{1}{R}\frac{dU}{dR} + \frac{d^2U}{dR^2}\right) + Mc(A_2\theta + A_3Qc\theta^2)cos(\alpha) - \frac{A_1U}{Da} - M = 0, \tag{85}$$

$$\frac{A_4}{Pr}\left(\frac{1}{R}\frac{d\theta}{dR} + \frac{d^2\theta}{dR^2}\right) + Q_T\theta + Q_Eexp(-nR) = 0, \tag{86}$$

$$\begin{aligned} &\text{at} \;\; R = 1: \;\; U = 0, \;\; \frac{d\theta}{dR} = \frac{Bi_1}{A_4}\theta, \\ &\text{at} \;\; R = \lambda: \;\; U = 0, \;\; \frac{d\theta}{dR} = \frac{Bi_2}{A_4}(1 - \theta). \end{aligned} \tag{87}$$

The physical quantities Nusselt number ($Nu_1$ & $Nu_\lambda$ ) and skin friction coefficient ($\tau_1$ & $\tau_\lambda$) at $R = 1$ and $R = \lambda$ are defined as:

$$\begin{aligned} &\text{at} \;\; R = 1: \;\; Nu_1 = \frac{k_{hnl}}{k_l}\left(\frac{d\theta}{dR}\right)_{R=1}, \;\; \tau_1 = \frac{\mu_{hnl}}{\mu_l}\left(\frac{dU}{dR}\right)_{R=1}, \\ &\text{at} \;\; R = \lambda: \;\; Nu_\lambda = -\frac{k_{hnl}}{k_l}\left(\frac{d\theta}{dR}\right)_{R=\lambda}, \;\; \tau_\lambda = -\frac{\mu_{hnl}}{\mu_l}\left(\frac{dU}{dR}\right)_{R=\lambda}. \end{aligned} \tag{88}$$

The nonlinear ordinary differential Eqns. (85)-(86) in view of boundary conditions (87) are solved numerically by using the finite difference method based bvp5c algorithm (see Shampine and Kierzenka [41]). The Nusselt number $Nu_1$ as compared with Oni [39] for various values of $Q_T$ ($Q_T = 0.5(0.5)3.0$). The comparison shows an excellent collaboration and offers confirmation to the validity of the present numerical solutions.

### 4.5.1 Parametric Analysis

The behavior of velocity $U(R)$, temperature $\theta(R)$, skin friction coefficients ($\tau_1$ & $\tau_\lambda$ ) and heat transfer rate ($Nu_1$ & $Nu_\lambda$) for change in values of effective parameters such as mixed convection parameter ($Mc$), quadratic convection parameter ($Qc$), angle of inclination ($\alpha$), temperature-related heat source parameter ($Q_T$), exponential space-related heat source parameter ($Q_E$), Darcy number ($Da$), Biot number for each cylinder ($Bi_1$ & $Bi_2$) and total nanoparticle volume fraction ($\phi$) are analyzed via graphs and tables. These graphs and tables are presented by fixing the effective parameters' values as $Mc = 2, Qc = 0.5, \alpha = \pi/4, Da = 0.1, Q_T = 0.01, Q_E = 0.1, Bi_1 = Bi_2 = 0.3, Pr = 6.0674$, and $\phi = 4\%$ unless otherwise stated (following Oni [39]).

### 4.5.2 Statistical Analysis

**Response surface methodology**

In this study, the RSM is performed to examine the least and most dominant input parameters influencing the response. Here the impact of input parameters $Q_T, Q_E$ and $\phi$ on the response $Nu_1$ is studied via RSM. The central composite design is one of the most commonly used second-order models (see Box and Wilson [23]). The reduced model for $Nu_1$ by eliminating the insignificant terms in Table 6 is given by:

$$\begin{aligned} Nu_1 =& 0.041832Q_T + 0.043398Q_E + 0.000823\phi + 0.005627Q_T^2 \\ &+ 0.005652Q_TQ_E + 0.293820. \end{aligned} \tag{89}$$

**Sensitivity analysis**

The partial derivatives of $Nu_1$ with respect to the key parameters $Q_T, Q_E$ and $\phi$ is termed as the sensitivity functions of $Nu_1$ to those key parameters. The sensitivity functions are given below:

$$\frac{\partial Nu_1}{\partial Q_T} = 0.041832 + 0.011254Q_T + 0.005652Q_E, \tag{90}$$

$$\frac{\partial Nu_1}{\partial Q_E} = 0.043398 + 0.005652Q_T, \tag{91}$$

$$\frac{\partial Nu_1}{\partial \phi} = 0.000823. \tag{92}$$

The sensitivity analysis for $Nu_1$ is performed by fixing $\phi$ at level 0 and changing the levels of ESHS and THS from -1 to +1.

### 4.5.3 Results

The nonlinear convective flow of hybrid nanoliquid in an inclined porous-annulus with an exponential space-related heat source and the temperature-dependent heat source is numerically simulated in the presence of convective boundary conditions. The main outcomes of this work are as below:

- The mechanisms of quadratic convection and mixed convection are favorable for the momentum of the hybrid nanoliquid.
- The velocity is less dominated by the acceleration due to gravity when the angle of inclination is increased.
- The magnitude of velocity and temperature fields has an increasing property for the exponential space-related heat source and temperature-dependent heat source phenomenon.
- The flow structure and thermal pattern at the outer cylinder enhance for an ascending value of Biot number, while the reverse trend is noticed at the inner cylinder.
- The momentum structure is higher in the porous region (Da$\neq$ 0) compared to the clear hybrid nanoliquid region ($Da = 0$)
- The velocity and temperature fields are greater for platelet-shaped nanoparticles followed by cylinder, brick, and spherical-shaped nanoparticles.
- The suspension of nanoparticles in the clear liquid is directly proportional to the temperature profile and inversely proportional to the velocity profile.
- The consequence of ESHS and THS are favorable for the heat transfer rate and friction factor.
- The mixed convection, Darcy number, and quadratic convection are positively related to the growth of the friction at the walls of the cylinders.
- The heat transport rate is dominated more by THS and less by the total nanoparticles volume fraction.
- The sensitivity of Nusselt number $Nu_1$ to the ESHS, THS, and concentration of nanoparticles are always positive.

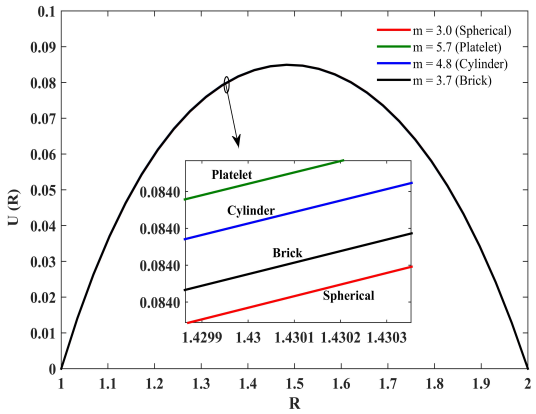


Figure 31: Impact of the shape of nanoparticles on $U(R)$.

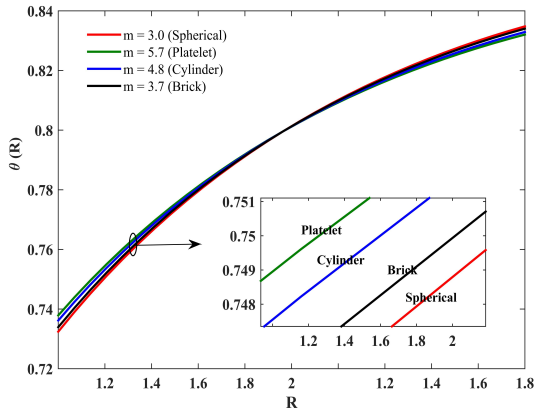


Figure 32: Impact of the shape of nanoparticles on $\theta(R)$.

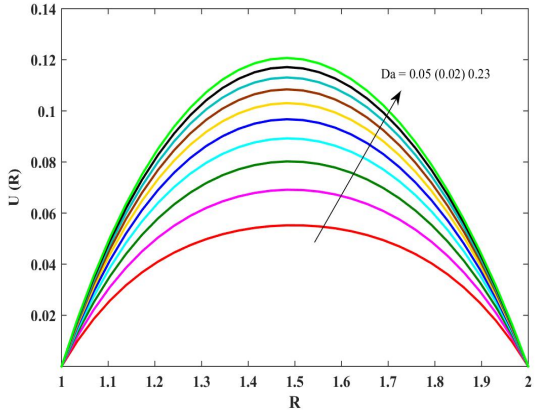


Figure 33: Impact of $Da$ on $U(R)$.

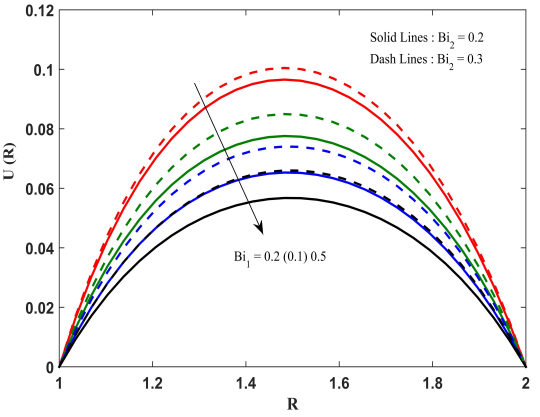


Figure 34: Impact of $Bi_1$ and $Bi_2$ on $U(R)$.

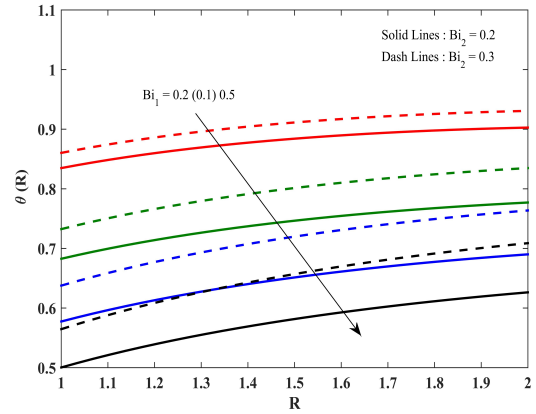


Figure 35: Impact of $Bi_1$ and $Bi_2$ on $\theta(R)$.

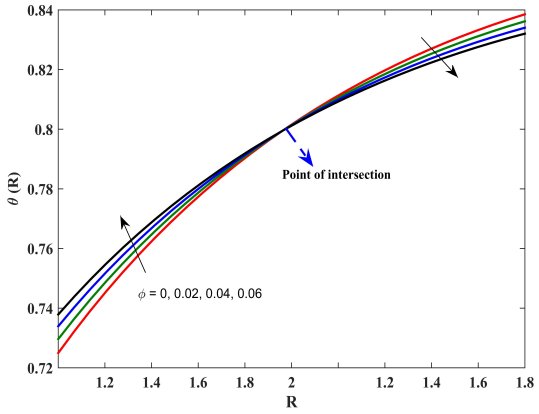


Figure 36: Impact of $\phi$ on $\theta(R)$.

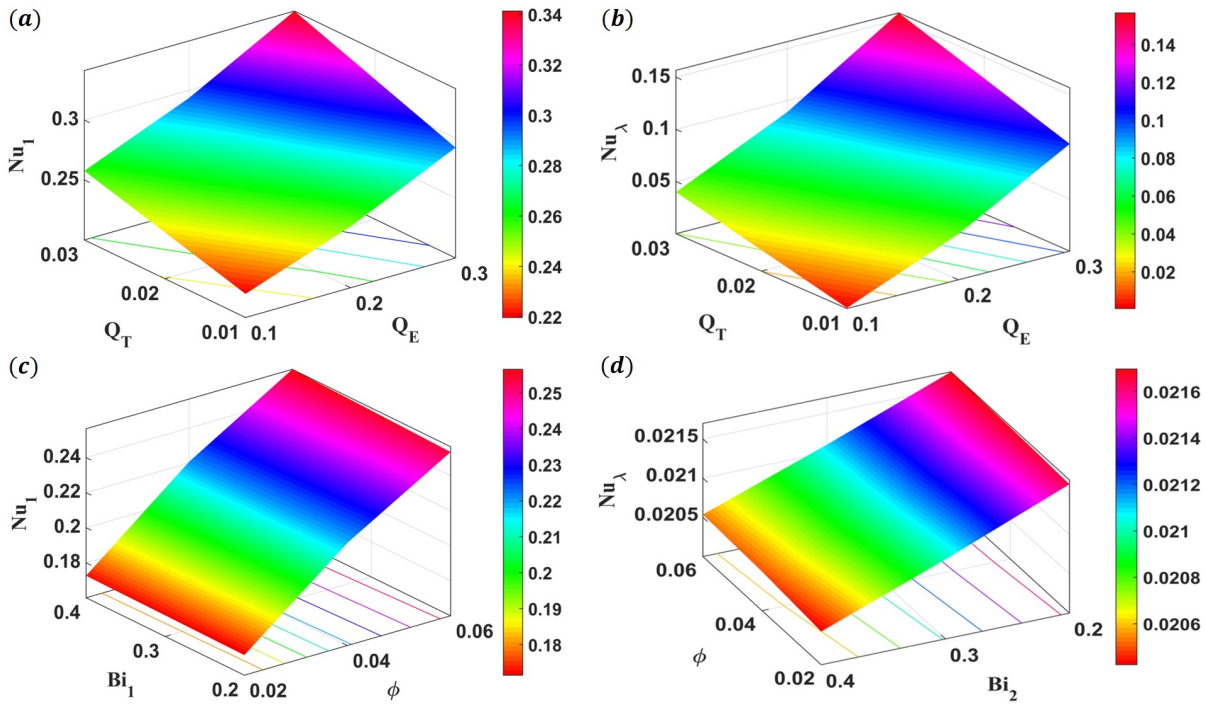


Figure 37: Impact of $Q_E, Q_T, \phi, Bi_1$ and $Bi_2$ on $Nu_1$ and $Nu_\lambda$.

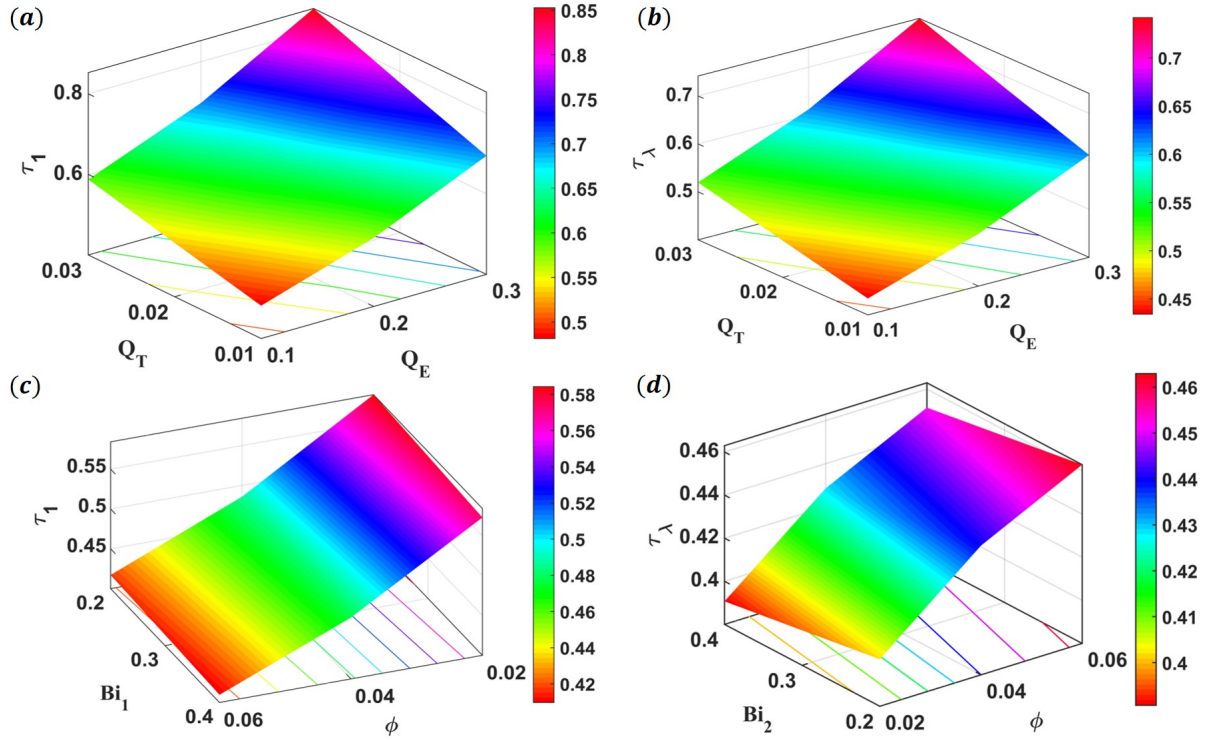


Figure 38: Impact of $Q_E, Q_T, \phi, Bi_1$ and $Bi_2$ on $\tau_1$ and $\tau_\lambda$.

## 4.6 PROBLEM 6: Flow of hybrid nanomaterial in an annulus using modified Buongiorno model

The physical model and the assumed coordinate system are considered as illustrated in Fig. 41. The horizontal annular conduit is filled with the water-based $Cu - Al_2O_3$ hybrid nanoliquid. The motion of hybrid nanoliquid is assumed to be non-transient, laminar, and incompressible. The modified Buongiorno model for the hybrid nanoliquid is considered along with the temperature-dependent heat source (THS), exponential space-related heat source (ESHS), and viscous dissipation phenomenon. A magnetic field of strength $B_0$ is applied at inclination angle $?^0$ with $z$-axis. The concentric cylinders of an outer radius $r_2$ and inner radius $r_1$, here the inner cylinder is rotated at a constant speed of $\Omega_1$ by fixing the outer cylinder. The surface of the inner cylinder is maintained at an unequal constant temperature $T_1$ and concentration $C_1$ while $T_2$ and $C_2$ at the outer cylinders (where $T_1 > T_2$ and $C_1 > C_2$). Enforcing the above hypothesizes, the governing equations in the dimensional form are given below (see Sheikholeslami and Rokni [42], Sheikholeslami and Abelman [43]):

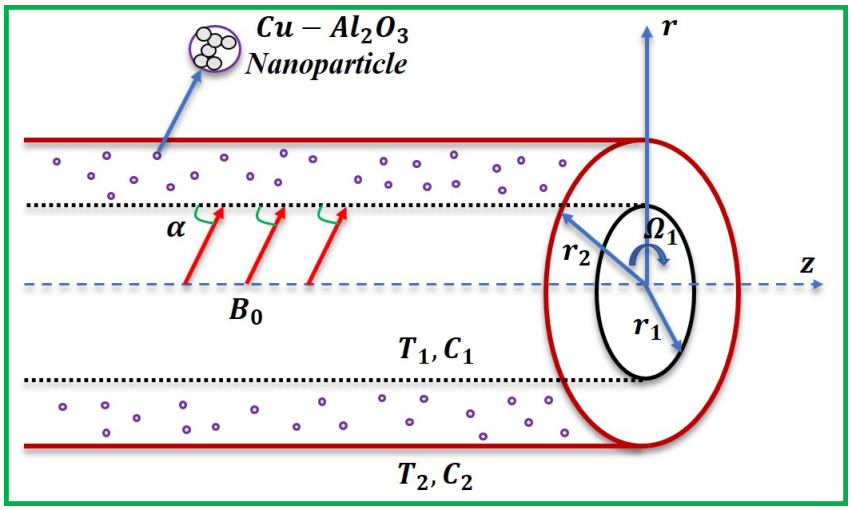


Figure 39: Physical model.

**The governing equations of the problem are:**

$$\rho_{hnl} v \frac{\partial v}{\partial r} = \mu_{hnl} \left( \frac{\partial^2 v}{\partial r^2} + \frac{1}{r}\frac{\partial v}{\partial r} - \frac{v}{r^2} \right) - \sigma_{hnl} B_0^2 v sin^2(\alpha), \tag{93}$$

$$(\rho C_p)_{hnl} v\frac{\partial T}{\partial r} = k_{hnl}\frac{1}{r}\frac{\partial}{\partial r}\left(r\frac{\partial T}{\partial r}\right) + \mu_{hnl}\left(\frac{\partial v}{\partial r} - \frac{v}{r}\right)^2 + (T - T_2)Qt + (T_1 - T_2)Q_e exp\left(-\frac{nr}{r_2}\right) + (\rho C_p)_{hp}\left[D_B\frac{\partial C}{\partial r}\frac{\partial T}{\partial r} + \frac{D_T}{T_1}\left(\frac{\partial T}{\partial r}\right)^2\right], \tag{94}$$

$$v\frac{\partial C}{\partial r} = \frac{D_B}{r}\frac{\partial}{\partial r}\left(r\frac{\partial C}{\partial r}\right) + \frac{D_T}{T_1}\frac{1}{r}\frac{\partial}{\partial r}\left(r\frac{\partial T}{\partial r}\right), \tag{95}$$

**Boundary conditions:**

$$\begin{aligned} &\text{at} \quad r = r_1 : \quad v(r) = \Omega_1 r_1, \quad C = C_1, \quad T = T_1, \\ &\text{at} \quad r = r_2 : \quad v(r) = 0, \quad C = C_2, \quad T = T_2. \end{aligned} \tag{96}$$

where $v$ denotes the velocity, $T, C, D_B, \alpha, D_T, Q_t, Q_e, n, \rho_{hnl}, k_{hnl}, (C_p)_{hnl}, \mu_{hnl}$ and $\sigma_{hnl}$ corresponds to temperature, nanoparticle concentration, Brownian motion coefficient $\left(= \frac{k_B T}{3\pi\mu_l(d_{Cu} + d_{Al_2O_3})}\right)$, an inclination angle of the magnetic field, thermophoretic coeffi-cient $\left(= 0.26\frac{k_l}{2k_l + (k_{Cu} + k_{Al_2O_3})}\frac{\mu_l}{\rho_l T}\phi\right)$, THS coefficient, ESHS coefficient, exponential index, density, thermal conductivity, specific heat at constant pressure, viscosity, and electrical conductivity coefficients. The subscript hp represents the hybrid particles.

The correlation for effective dynamic viscosity and thermal conductivity of water-based $Cu - Al_2O_3$ hybrid nanoliquid is taken from the experimental work of Corcione [44] and are as follows:

$$\frac{\mu_{hnl}}{\mu_l} = \frac{1}{1 - 34.87 d_f^{0.3}[d_{Cu}^{-0.3}\phi_{Cu}^{1.03} + d_{Al_2O_3}^{-0.3}\phi_{Al_2O_3}^{1.03}]}, \tag{97}$$

$$k_{hnl}k_l = 1 + \frac{4.4 Re_B^{0.4} Pr^{0.66}\left(\frac{T}{T_{fr}}\right)^{10}[k_{Cu}^{0.03}\phi_{Cu}^{0.66} + k_{Al_2O_3}^{0.03}\phi_{Al_2O_3}^{0.66}]}{k_f^{0.03}}, \tag{98}$$

$$Re_B = \frac{2k_b T\rho_l}{\pi\mu_l^2(d_{Cu} + d_{Al_2O_3})}. \tag{99}$$

here $d_{Cu}$=25nm and $Al_2O_3$=28nm (nanoparticle diameter), $d_f = 3.85\times10^{-10}$ m (molecule diameter of the base liquid), the nanoparticle volume fraction ranges between $2\% < \phi < 9\%$, $T_{fr} = 273.15$ K (freezing point of base liquid), $T$=300K, $k_b = 1.3807 \times 10^{-23} JK^{-1}$ (Boltzmann's constant).

The effective thermophysical properties of water-based $Cu-Al_2O_3$ hybrid nanoliquid are as follows (see Goudarzi et al. [45])

$$\rho_{hnl} = \left[(1-\phi) + \frac{(\phi\rho)_{Cu}}{\rho_l} + \frac{(\phi\rho)_{Al_2O_3}}{\rho_l}\right]\rho_l,$$

$$(\rho C_p)_{hnl} = \left[(1-\phi) + \frac{\phi_{Cu}(\rho C_p)_{Cu}}{(\rho C_p)_l} + \frac{\phi_{Al_2O_3}(\rho C_p)_{Al_2O_3}}{(\rho C_p)_l}\right](\rho C_p)_l,$$

$$\sigma_{hnl} = \sigma_l\left[1 + \frac{3(\sigma_{Cu}-1)\phi_{Cu}}{\sigma_{Cu}+2-(\sigma_{Cu}-1)\phi_{Cu}}\right]\left[1 + \frac{3(\sigma_{Al_2O_3}-1)\phi_{Al_2O_3}}{\sigma_{Al_2O_3}+2-(\sigma_{Al_2O_3}-1)\phi_{Al_2O_3}}\right],$$

$$\phi = \phi_{Cu} + \phi_{Al_2O_3},$$

$$C_{p,hp} = \frac{\phi_{Cu}C_{p,Cu} + \phi_{Al_2O_3}C_{p,Al_2O_3}}{\phi}, \tag{100}$$

Introducing the following dimensionless quantities along with the thermophysical properties of hybrid nanoliquid:

$$R = \frac{r}{r_2}, \quad V = \frac{v}{\Omega_1 r_1}, \quad \eta = \frac{r_1}{r_2}, \quad \triangle C = C_1 - C_2,$$
$$\theta = \frac{T-T_2}{T_1-T_2}, \quad S = \frac{C-C_2}{C_1-C_2}, \quad \triangle T = T_1 - T_2. \tag{101}$$

Eqns. (93)-(96) takes the form as follows:

$$\frac{d^2V}{dR^2} + \frac{1}{R}\frac{dV}{dR} - \left[\frac{1}{R^2} + \frac{A_3}{A_2}\frac{Ha^2}{(1-\eta)^2}sin^2\alpha\right]V - \frac{A_1}{A_2}ReV\frac{dV}{dR} = 0, \tag{102}$$

$$\frac{1}{Pr}\frac{1}{R}\frac{d}{dR}\left(R\frac{d\theta}{dR}\right) + \frac{A_2}{A_5}E_c\left(\frac{dV}{dR} - \frac{V}{R}\right)^2 + \frac{Q_T}{A_5}\theta - \frac{A_4}{A_5}ReV\frac{d\theta}{dR} + \frac{Q_E}{A_5}exp(-nR)$$
$$+ \frac{1}{Pr}\frac{Nb}{A_5}\frac{dS}{dR}\frac{d\theta}{dR} + \frac{1}{Pr}\frac{Nt}{A_5}\left(\frac{d\theta}{dR}\right)^2 = 0, \tag{103}$$

$$\frac{1}{R}\frac{d}{dR}\left(R\frac{dS}{dR}\right) + \frac{Nt}{Nb}\frac{1}{R}\frac{d}{dR}\left(r\frac{d\theta}{dR}\right) - ReScV\frac{dS}{dR} = 0, \tag{104}$$

$$\begin{aligned} &\text{at} \quad R=\eta: \quad V(\eta)=1, \quad S(\eta)=1, \quad \theta(\eta)=1, \\ &\text{at} \quad R=1: \quad V(1)=0, \quad S(1)=0, \quad \theta(1)=0. \end{aligned} \tag{105}$$

The physical quantities Nusselt number and Sherwood number at $R=\eta$ and $R=1$ are as follows (see Sheikholeslami and Abelman [43]): At inner cylinder:

$$Nu_i = -\frac{k_{hnl}}{k_l}(1-\eta)\theta^{'}(\eta), \qquad Sh_i = -(1-\eta)S^{'}(\eta), \tag{106}$$

At outer cylinder:

$$Nu_o = -\frac{k_{hnl}}{k_l}(1-\eta)\theta^{'}(1), \qquad Sh_o = -(1-\eta)S^{'}(1). \tag{107}$$

where $Re = \dfrac{\rho_l \Omega_1 r_1 r_2}{\mu_l}$ is Reynolds number, $Ec = \dfrac{\rho_l(\Omega_1 r_1)^2}{(\rho C_p)_l \triangle T}$ is Eckert number, $Pr = \dfrac{\mu_l(\rho C_p)_l}{\rho_l k_l}$ is Prandtl number, $Q_T = \dfrac{r_2^2 Q_t}{\nu_l(\rho C_p)_l}$ is THS parameter, $Q_E = \dfrac{r_2^2 Q_e}{\nu_l(\rho C_p)_l}$ is ESHS parameter, $Ha = B_0(r_2-r_1)\sqrt{\left(\dfrac{\sigma_l}{\mu_l}\right)}$ is Hartmann number, $Nb = \dfrac{(\rho C_p)_{hp} D_B \triangle C}{k_l}$ is Brownian motion parameter, $Nt = \dfrac{(\rho C_p)_{hp} D_T \triangle T}{T_1 k_l}$ is thermophoresis parameter, $Sc = \dfrac{\mu_l}{\rho_l D_B}$ is Schmidt number, $\alpha$ is the inclination angle of the magnetic field and $\eta$ is the radius ratio.

Before employing the finite difference method based on the bvp4c algorithm, the system of nonlinear differential Eqns. (102)-(105) are converted into a system of first-order differential equations (ODEs). These nonlinear ODEs subjected to initial conditions are solved using the bvp4c routine in MATLAB. Here the values for the initial guess are approximated until the boundary conditions are satisfied. Besides, the maximum residuals are set to $10^{-5}$.

### 4.6.1 Parametric Analysis

The behaviour of velocity $V(R)$, temperature $\theta(R)$ and concentration $S(R)$ profiles for change in the values of curious key parameters of the current study are Hartmann number $Ha$, inclination angle of the magnetic field $\alpha$, Reynolds number $Re$, total nanoparticle volume fraction $\phi$, temperature-dependent heat source $Q_T$, exponential space-related heat source $Q_E$, Schmidt number $Sc$, Eckert number $Ec$, Brownian motion parameter $Nb$, and thermophoretic parameter $Nt$ are visualized through two-dimensional (2D) and three-dimensional (3D) surface plots. For numerical computation the prescribed data values are $Ec = 0.01, \alpha = \pi/4, Re = 1, Ha = 2, Q_T = 0.5, Nb = Nt = 0.1, Q_E = 1.5, Le = 3, \phi = 2\%$ and $Pr = 6.0674$ (unless otherwise stated), these values are extracted

from the literature Sheikholeslami and Abelman [43], Tassaddiq et al. [46]. Further, the Nusselt number and Sherwood numbers are optimized using the response surface methodology (RSM) to understand the heat and mass transport in a more elegant way.

### 4.6.2 Statistical Analysis

**Response surface methodology**

The main objective of this procedure is to optimize the dependent variable (response) that is affected by several independent variables. The RSM is employed to extract the model for Nusselt number (response) and to find the dominant effect. This approach designs the test matrix by considering the number of variables (chosen effective parameters are $Re, Nt, Nb$) as well as maximum and minimum limits specified for each variable. The reduced model for $Nu_i$ by considering only the significant terms in ANOVA yield:

$$\begin{aligned} Nu_i = &- 0.176056Re - 0.009146Nt - 0.045278Nb + 0.018740Re^2 + 0.000981Nb^2 \\ &+ 0.001888ReNt + 0.009663ReNb + 0.000405NtNb + 0.374671. \end{aligned} \tag{108}$$

**Sensitivity analysis**

Sensitivity analysis is another important aspect that analyzes how the small variation in the value of the effective parameters under certain conditions affects the response variable. An enhancing or declining trend of the response ($Nu_i$) with respect to $Re, Nt$ and $Nb$ can be computed from the sensitivity functions derived as follows:

$$\frac{\partial Nu_i}{\partial Re} = -0.176056 + 0.037480Re + 0.001888Nt + 0.009663Nb, \tag{109}$$

$$\frac{\partial Nu_i}{\partial Nt} = -0.009146 + 0.001888Re + 0.000405Nb, \tag{110}$$

$$\frac{\partial Nu_i}{\partial Nb} = -0.045278 + 0.001962Nb + 0.009663Re + 0.000405Nt. \tag{111}$$

The numerical values are obtained for $Nu_i$ with $Nt$ at level 0, $Nb$ & $Re$ with levels of -1, 0, +1.

### 4.6.3 Results

The system of nonlinear differential equations governing the flow of hybrid nanoliquid with the modified Buongiorno model is numerically simulated in the presence of inclined

magnetic field, temperature-dependent heat source and exponential space-related heat source aspect. The main outcomes of this study are:

- The velocity field has an inverse association with the applied magnetic field and its angle of inclination.
- The exponential space-related heat source and temperature-related heat source mechanisms are directly proportional to the growth of the thermal pattern.
- The chaotic motion of nanoparticles advances the thickness of the thermal and solutal boundaries.
- The thermal migration of nanoparticles declines the magnitude of concentration profile.
- The flow structure and concentration profile augment with the addition of nanoparticles, implying that more collision between the dispersed nanoparticles.
- The consequence of the Reynolds number is favorable for the velocity and temperature fields.
- The heat transport rate at the inner cylinder strengthened upon intensifying the ESHS, THS, Reynolds number, and thermophoretic aspect.
- The Lewis number, applied magnetic field, Brownian motion, and total nanoparticle volume fraction enhance the mass transport rate at the inner cylinder.
- The heat transport is more dominated by the Reynolds number compared to the chaotic motion of nanoparticles and thermophoretic aspect.
- The sensitivity of Nusselt number $Nu_i$ to the Reynolds number, chaotic motion of nanoparticles and thermophoretic aspect are always negative.

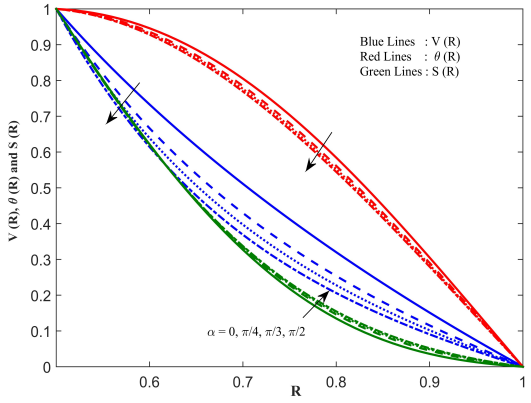


Figure 40: Consequence of $\alpha$ on $V(R)$, $\theta(R)$ and $S(R)$.

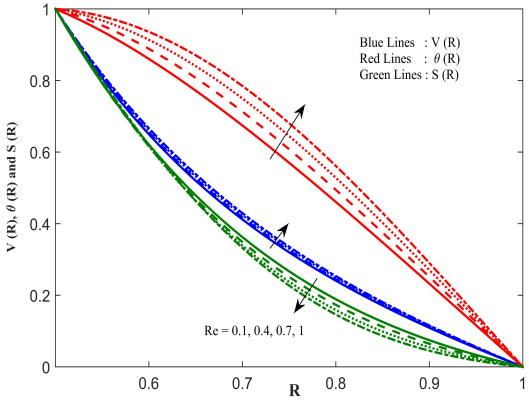


Figure 41: Consequence of $Re$ on $V(R)$, $\theta(R)$ and $S(R)$.

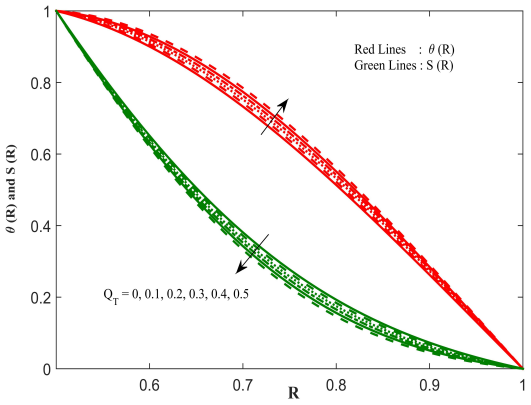


Figure 42: Consequence of $Q_T$ on $\theta(R)$ & $S(R)$.

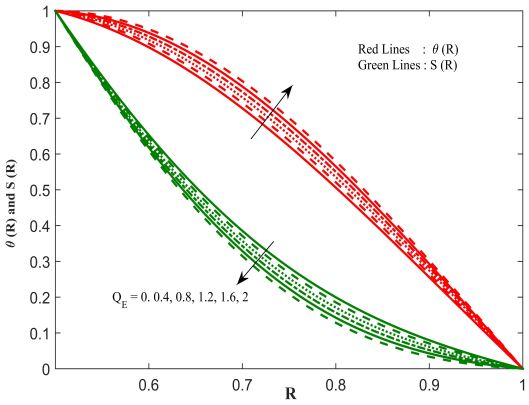


Figure 43: Consequence of $Q_E$ on $\theta(R)$ & $S(R)$.

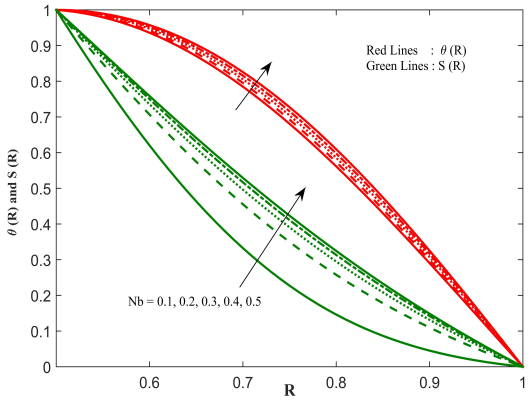


Figure 44: Consequence of $Nb$ on $\theta(R)$ & $S(R)$.

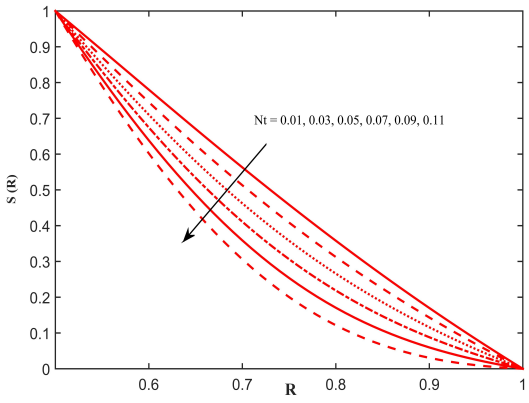


Figure 45: Consequence of $Nt$ on $S(R)$.

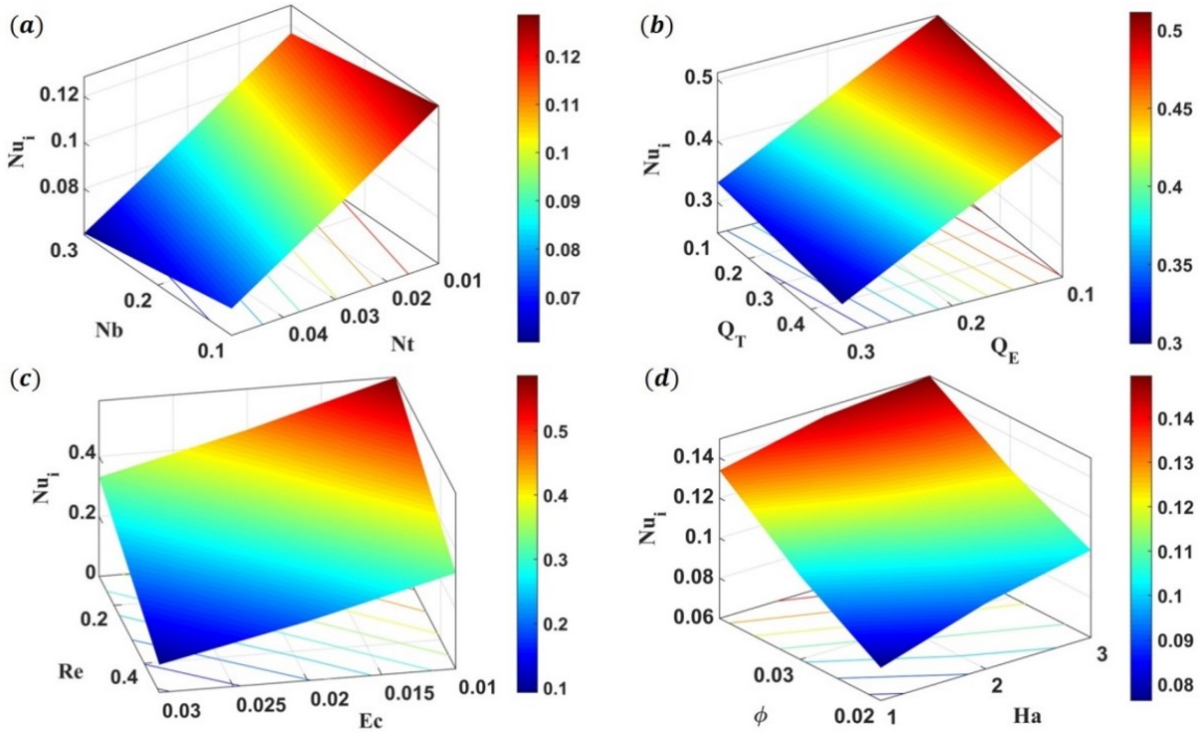


Figure 46: Consequence of $Nt, Nb, Q_T, Q_E, Re, Ec, \phi$ & $Ha$ on $Nu_i$.

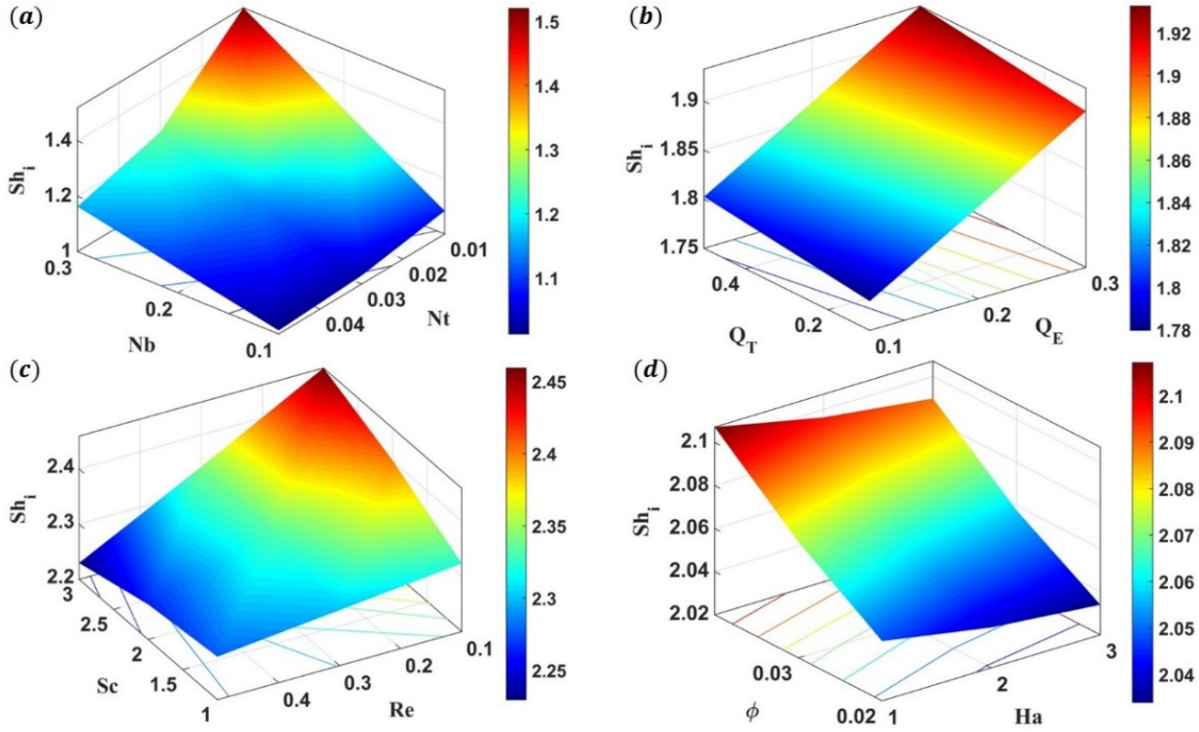


Figure 47: Consequence of $Nt, Nb, Q_T, Q_E, Re, Sc, \phi$ & $Ha$ on $Sh_i$.

# 5 STRUCTURE OF THE DISSERTATION

The dissertation is organised as follows:

**Problem 1:** This study investigate the momentum and thermal behavior of the radiated flow of magneto-hybrid nanoliquid ($Cu - Al_2O_3 - H_2O$) in an annulus with moving walls under nonlinear Boussinesq approximation (NBA).

**Problem 2:** The main goal of this study is to scrutinize the mutual impact of nonlinear convection and nonlinear thermal radiative flow of magneto-hybrid nanoliquid in an annulus with exponential space related heat source/sink aspect.

**Problem 3:** The significance of variable thermal conductivity and viscosity on the heat transport characteristics of water-based $Ag - MgO$ hybrid nanoliquid in a vertical micro-annulus exposed to quadratic convection, velocity slip and temperature jump boundary conditions is examined in this study.

**Problem 4:** Heat transport characteristics of the hybrid nanoliquid (HNL) in an upright annulus exposed to quadratic convection and non-uniform heat source/sink using response surface methodology have been analysed in this problem.

**Problem 5:** This work through light on dynamics of hybrid nanoliquids in an inclined porous-annulus employing nonlinear Boussinesq approximation, temperature-dependent heat source (THS), and exponential space-dependent heat source (ESHS) aspects, where the surface of the inner and outer cylinders is exposed to convective boundary condition.

**Problem 6:** This study highlights the heat and mass transport characteristics of hybrid nanoliquid ($Cu - Al_2O_3 - H_2O$) in a horizontal annulus using modified Buongiorno model. Inclined magnetisum, viscous dissipation and the two different heat sources, namely the temperature-related heat source (THS) & the space-related exponential heat source (ESHS) aspects, are also considered in this study.

# 6 FUTURE RESEARCH WORK

The study of heat transport characteristics of hybrid nanofluids in an annulus utilizing nonlinear Boussnesqe approximation is still in its initial phase. There is a lot of work to be done in this area. In the future, the mathematical models provided in this study can be expanded in the following directions:

- Optimizing the heat and mass transport rate of hybrid nanofluids including non-New -tonian fluids models.

- The flow geometry can be considered in the form of a parallel rotating plate, disk, or cylinder to further increase the applications of the present research.

# References


[1] S. L. Goren, "On free convection in water at 4 c," *Chemical EngineeringScience*, vol. 21, no. 6-7, pp. 515-518, 1966.

[2] K. Vajravelu and K. S. Sastri, "Fully developed laminar free convection flowbetween two parallel vertical walls-I," *International Journal of Heat andMass Transfer*, vol. 20, no. 6, pp. 655-660, 1977.

[3] P. K. Kameswaran, B. Vasu, P. V. S. N. Murthy, and R. S. R. Gorla, "Mixed convection from a wavy surface embedded in a thermally stratified nanofluidsaturated porous medium with non-linear Boussinesq approximation," *International Communications in Heat and Mass Transfer*, vol. 77, pp. 78-86,2016.

[4] B. Mahanthesh, B. J. Gireesha, G. T. Thammanna, S. A. Shehzad, F. M. Abbasi, and R. S. R. Gorla, "Nonlinear convection in nano maxwell fluid with nonlinear thermal radiation: A three-dimensional study," *Alexandria Engineering Journal*, vol. 57, no. 3, pp. 1927-1935, 2018.

[5] B. J. Gireesha, P. S. Kumar, B. Mahanthesh, S. A. Shehzad, and F. M. Abbasi, "Nonlinear gravitational and radiation aspects in nanoliquid with exponential space dependent heat source and variable viscosity," *Microgravity Science and Technology*, vol. 30, no. 3, pp. 257-264, 2018.

[6] B. Vasu, R. S. R. Gorla, O. A. Bég, P. V. S. N. Murthy, V. R. Prasad, and A. Kadir, "Unsteady flow of a nanofluid over a sphere with nonlinear boussinesq ap-proximation," *Journal of Thermophysics and Heat Transfer*, vol. 33, no. 2,pp. 343-355, 2019.

[7] B. K. Jha and M. N. Sarki, "Chemical reaction and dufour effects on non-linear free convection heat and mass transfer flow near a vertical movingporous plate," *Heat Transfer*, vol. 49, no. 2, pp. 984-999, 2020.

[8] S. U. Choi and J. A. Eastman, "Enhancing thermal conductivity of fluids with nanoparticles,"Argonne National Lab., IL (United States), Tech.Rep., 1995.

[9] K. Khanafer, K. Vafai, and M. Lightstone, "Buoyancy-driven heat transfer enhancement in a two-dimensional enclosure utilizing nanofluids," *International Journal of Heat and Mass Transfer*, vol. 46, no. 19, pp. 3639-3653, 2003.

[10] J. Buongiorno, "Convective transport in nanofluids," *ASME*, vol. 128, no. 3, pp. 240-250, 2006.

[11] S. Suresh, K. P. Venkitaraj, P. Selvakumar, and M. Chandrasekar, "Effect of $Al_2O_3$-$Cu$/water hybrid nanofluid in heat transfer," *Experimental Thermaland Fluid Science*, vol. 38, pp. 54-60, 2012.

[12] S. A. Devi and S. S. U. Devi, "Numerical investigation of hydromagnetic hybrid $Cu - Al_2O_3$/water nanofluid flow over a permeable stretching sheet with suction," *International Journal of Nonlinear Sciences and Numerical Simulation*, vol. 17, no. 5, pp. 249-257, 2016.

[13] S. Amala and B. Mahanthesh, "Hybrid nanofluid flow over a vertical rotating plate in the presence of hall current, nonlinear convection and heatabsorption," *Journal of Nanofluids*, vol. 7, no. 6, pp. 1138-1148, 2018.

[14] S. Nadeem, N. Abbas, and A. U. Khan, "Characteristics of three dimensional stagnation point flow of hybrid nanofluid past a circular cylinder," *Results in physics*, vol. 8, pp. 829-835, 2018.

[15] B. Mahanthesh, "Statistical and exact analysis of mhd flow due to hybridnanoparticles suspended in $C_2H_6O_2 - H_2O$ hybrid base fluid," *Mathematical Methods in Engineering and Applied Sciences (CRC Press, 2020)*, pp. 185-228, 2020.

[16] D. A. Nield, A. Bejan "Convection in porous media,"Springer, vol. 3, 2006.

[17] D. B. Ingham and I. Pop, "Transport phenomena in porous media III,"Elsevier, vol. 3, 2005.

[18] T. Paul and A. K. Singh, "Natural convection between coaxial vertical cylinders partially filled with a porous material," *Forschung im Ingenieurwesen*,vol. 64, no. 6-7, pp. 157-162, 1998.

[19] B. K. Jha and M. O. Oni, "Transient natural convection flow between vertical concentric cylinders heated/cooled asymmetrically," *Proceedingsof the Institution of Mechanical Engineers, Part A: Journal of Power and Energy*, vol. 232, no. 7, pp. 926-939, 2018.

[20] A. Shakiba and A. B. Rahimi, "Nanofluid flow and MHD mixed convection inside a vertical annulus with moving walls and transpiration considering the effect of brownian motion and shape factor," *Journal of Thermal Analysis and Calorimetry*, vol. 138, no. 1, pp. 501-515, 2019.

[21] B. K. Jha and M. O. Oni, "Role of magnetic field on mixed convective flow between two concentric microtubes with heat generation/absorption:an exact solution," *Proceedings of the Institution of Mechanical Engineers,Part N: Journal of Nanomaterials, Nanoengineering and Nanosystems*, vol.232, no. 2-3, pp. 59-67, 2018.

[22] F. Mebarek-Oudina, A. Aissa, B. Mahanthesh, and H. F. Öztop, "Heat transport of magnetized newtonian nanoliquids in an annular space between porous vertical cylinders with discrete heat source," *International Communications in Heat and Mass Transfer*, vol. 117, p. 104737, 2020.

[23] G. E. Box and K. B. Wilson, "On the experimental attainment of optimum conditions," *Journal of the royal statistical society: Series B (Methodological)*, vol. 13, no. 1, pp. 1-38, 1951.

[24] R. H. Myers, A. I. Khuri, and W. H. Carter, "Response surface methodology: 1966-l988," *Technometrics*, vol. 31, no. 2, pp. 137-157, 1989.

[25] M. Akbarzadeh, S. Rashidi, M. Bovand, and R. Ellahi, "A sensitivity analysis on thermal and pumping power for the flow of nanofluid inside a wavy channel," *Journal of Molecular Liquids*, vol. 220, pp. 1-13, 2016.

[26] M. Mamourian, K. M. Shirvan, and S. Mirzakhanlari, "Two phase simulation and sensitivity analysis of effective parameters on turbulent combined heat transfer and pressure drop in a solar heat exchanger filled with nanofluid by response surface methodology," *Energy*, vol. 109, pp. 49-61,2016.

[27] A. H. Pordanjani, S. M. Vahedi, F. Rikhtegar, and S. Wongwises, "Optimization and sensitivity analysis of magneto-hydrodynamic natural convection nanofluid flow inside a square enclosure using response surface methodology," *Journal of Thermal Analysis and Calorimetry*, vol. 135, no. 2, pp.1031-1045, 2019.

[28] S. M. Vahedi, A. H. Pordanjani, A. Raisi, and A. J. Chamkha, "Sensitivity analysis and optimization of MHD forced convection of a $Cu$-water nanofluidflow past a wedge," *The European Physical Journal Plus*, vol. 134, no. 3, pp. 1-21, 2019.

[29] B. Mahanthesh and J. Mackolil, "Flow of nanoliquid past a vertical plate with novel quadratic thermal radiation and quadratic Boussinesq approximation: sensitivity analysis," *International Communications in Heat and Mass Transfer*, vol. 120, p. 105040, 2021.

[30] B. K. Jha, B. Aina, and Z. Rilwanu, "Steady fully developed natural convection flow in a vertical annular microchannel having temperature dependent viscosity: an exact solution," *Alexandria Engineering Journal*, vol. 55,no. 2, pp. 951-958, 2016.

[31] H. C. Weng, "Drag reduction and heat transfer enhancement over a heated wall of a vertical annular microchannel," *International Journal of Heat and Mass Transfer*, vol. 52, no. 3-4, pp. 1075-1079, 2009.

[32] M. H. Esfe, A. A. A. Arani, M. Rezaie, W. M. Yan, and A. Karimipour,"Experimental determination of thermal conductivity and dynamic viscosity of $Ag - MgO$/water hybrid nanofluid," *International Communications in Heat and Mass Transfer*, vol. 66, pp. 189-195, 2015.

[33] F. C. Lai and F. A. Kulacki, "The effect of variable viscosity on convective heat transfer along a vertical surface in a saturated porous medium," *International Journal of Heat and Mass Transfer*, vol. 33, no. 5, pp. 1028-1031,1990.

[34] K. Vajravelu, K. V. Prasad, R. A. Van Gorder, and J. Lee, "Free convection boundary layer flow past a vertical surface in a porous medium with temperature-dependent properties," *Transport in Porous Media*, vol. 90,no. 3, pp. 977-992, 2011.

[35] T. C. Chiam, "Heat transfer with variable conductivity in a stagnation-point flow towards a stretching sheet," *International Communications in Heat and Mass Transfer*, vol. 23, no. 2, pp. 239-248, 1996.

[36] D. Kumar and A. K. Singh, "Effects of heat source/sink and induced magnetic field on natural convective flow in vertical concentric annuli," *Alexandria Engineering Journal*, vol. 55, no. 4, pp. 3125-3133, 2016.

[37] R. K. Singh and A. K. Singh, "Effect of induced magnetic field on natural convection in vertical concentric annuli," *Acta Mechanica Sinica*, vol. 28, no. 2,pp. 315-323, 2012.

[38] I. Shahzadi and S. Nadeem, "Inclined magnetic field analysis for metallic nanoparticles submerged in blood with convective boundary condition," *Journal of Molecular Liquids*, vol. 230, pp. 61-73, 2017.

[39] M. O. Oni, "Combined effect of heat source, porosity and thermal radiationon mixed convection flow in a vertical annulus: An exact solution," *Engineering Science and Technology, an International Journal*, vol. 20, no. 2,pp. 518-527, 2017.

[40] D. Srinivasacharya and K. H. Bindu, "Entropy generation due to micropolar fluid flow between concentric cylinders with slip and convective boundary conditions," *Ain Shams Engineering Journal*, vol. 9, no. 2, pp. 245-255, 2018.

[41] J. Kierzenka and L. F. Shampine, "A BVP solver based on residual control and the MATLAB PSE," *ACM Transactions on Mathematical Software(TOMS)*, vol. 27, no. 3, pp. 299-316, 2001.

[42] M. Sheikholeslami and H. B. Rokni, "Influence of melting surface on MHD nanofluid flow by means of two phase model," *Chinese Journal of Physics*,vol. 55, no. 4, pp. 1352-1360, 2017.

[43] M. Sheikholeslami and S. Abelman, "Two-phase simulation of nanofluid flow and heat transfer in an annulus in the presence of an axial magnetic field," *IEEE Transactions on Nanotechnology*, vol. 14, no. 3, pp. 561-569,2015.

[44] M. Corcione, "Empirical correlating equations for predicting the effective thermal conductivity and dynamic viscosity of nanofluids," *Energy Conversion and Management*, vol. 52, no. 1, pp. 789-793, 2011.

[45] S. Goudarzi, M. Shekaramiz, A. Omidvar, E. Golab, A. Karimipour, and A. Karimipour, "Nanoparticles migration due to thermophoresis and brownian motion and its impact on $Ag - MgO$/water hybrid nanofluid natural convection," *Powder Technology*, vol. 375, pp. 493-503, 2020.

[46] A. Tassaddiq, S. Khan, M. Bilal, T. Gul, S. Mukhtar, Z. Shah, and E. Bonyah, "Heat and mass transfer together with hybrid nanofluid flow over a rotating disk," *AIP Advances*, vol. 10, no. 5, pp. 055317, 2020.

# LIST OF PUBLICATIONS

1. K. Thriveni, and B. Mahanthesh, "Optimization and sensitivity analysis of heat transport of hybrid nanoliquid in an annulus with quadratic Boussinesq approximat -ion and quadratic thermal radiation", *The European Physical Journal Plus*, vol. 135(6), pp. 1-22, 2020.

2. K. Thriveni, and B. Mahanthesh, "Nonlinear Boussinesq buoyancy driven flow and radiative heat transport of magnetohybrid nanoliquid in an annulus: A statistical framework", *Heat Transfer*, vol. 49(8), pp. 4759-4782, 2020.

3. K. Thriveni, and B. Mahanthesh, "Sensitivity analysis of nonlinear radiated heat transport of hybrid nanoliquid in an annulus subjected to the nonlinear Boussinesq approximation", *Journal of Thermal Analysis and Calorimetry*, vol. 143(3), pp. 2729-2748, 2021.

4. K. Thriveni, and B. Mahanthesh, "Significance of variable fluid properties on hybrid nanoliquid flow in a micro-annulus with quadratic convection and quadratic thermal radiation: Response Surface Methodology", *International Communications in Heat and Mass Transfer*, vol. 124, pp. 105264, 2021.

5. K. Thriveni, and B. Mahanthesh, "Heat transport of hybrid nanomaterial in an annulus with quadratic Boussinesq approximation", *Applied Mathematics and Mech--anics (English Edition)*, vol. 42, pp. 885-900, 2021.

6. K. Thriveni, and B. Mahanthesh, "Nonlinear convective flow and heat transfer of hybrid nanomaterial between two concentric cylinders with convective thermal condition and exponential heat source", *International Communications in Heat and Mass Transfer*, (**Under review**).

7. "Response Surface optimization of hybrid nanomaterial heat flow in an annulus with internal heat sources: Modified Buongiorno model", (**Yet to submit**).

# LIST OF PRESENTATIONS

- Presented a paper entitled "Nonlinear Boussinesq buoyancy driven flow and radiative heat transport of magneto-hybrid nanoliquid in an annulus: A statistical framework" in International Conference on Emerging Trends in Fluid Mechanics and its Applicati--ons (ICETFMA-2020), held at Department of Mathematics, CHRIST (Deemed to be University), Bengaluru during 27-28 February 2020.

- Presented a paper entitled "Optimization and sensitivity analysis of heat transport of hybrid nanoliquid in an annulus with quadratic Boussinesq approximation and quadratic thermal radiation" in the International Conference on Emerging Trends in Mathematics and Statistics (ICETMS-2020 online) during 21-23, October 2020 organized by Post Graduate Department of Mathematics & Statistics and IQAC, St. George's College Aruvithura, Kottayam in association with Kerala Mathematical Association (KMA).

- Presented a paper entitled "Sensitivity analysis of nonlinear radiated heat transport of hybrid nanoliquid in an annulus subjected to the nonlinear Boussinesq approximat--ion" in the $65^{th}$ congress of ISTAM (International Conference) during 9-11, December 2020 organized by GITAM Deemed to be University, Hyderabad.